KAUNAS UNIVERSITY OF TECHNOLOGY

ALGIMANTAS IVANAUSKAS

FORMATION AND STUDY OF COPPER AND INDIUM SELENIDES LAYERS ON GLASS USING SELENOPOLYTHIONATE ACIDS

Doctoral dissertation
Physical Sciences, Chemistry (03P)

2018, Kaunas

This doctoral dissertation was prepared at Kaunas University of Technology, Faculty of Chemical Technology, Department of Physical and Inorganic Chemistry during the period of 2012–2017.

Scientific Supervisor:

Prof. Dr. Ingrida ANCUTIENĖ (Kaunas University of Technology, Physical Sciences, Chemistry – 03P).

Doctoral dissertation has been published in:
http://ktu.edu

English Language Editor:

Dovilė Dumbrauskaitė (Publishing Office "Technologija").

Lithuanian Language Editor:

Aurelija Gražina Rukšaitė (Publishing Office "Technologija").

ISBN 978-609-02-1423-7

The bibliographical information of this issue is available at Martynas Mazvydas National Library of Lithuania National Bibliographic Database (NBD)

KAUNO TECHNOLOGIJOS UNIVERSITETAS

ALGIMANTAS IVANAUSKAS

VARIO IR INDŽIO SELENIDŲ SLUOKSNIŲ ANT STIKLO GAVIMAS NAUDOJANT SELENOPOLITIONATŲ RŪGŠTIS

Daktaro disertacija
Fiziniai mokslai, chemija (03P)

2018, Kaunas

Disertacija rengta 2012–2017 metais Kauno technologijos universiteto cheminės technologijos fakultete fizikinės ir neorganinės chemijos katedroje.

Mokslinis vadovas:

Prof. dr. Ingrida ANCUTIENĖ (Kauno technologijos universitetas, fiziniai mokslai, chemija – 03P).

Interneto svetainės, kurioje skelbiama disertacija, adresas:
http://ktu.edu

Anglų kalbą redagavo:

Dovilė Dumbrauskaitė (Leidykla "Technologija").

Lietuvių kalbą redagavo:

Aurelija Gražina Rukšaitė (Leidykla "Technologija").

ISBN 978-609-02-1423-7

Leidinio bibliografinė informacija pateikiama Lietuvos nacionalinės Martyno Mažvydo bibliotekos Nacionalinės bibliografijos duomenų banke (NBDB)

TABLE OF CONTENTS

SYMBOLS AND ABBREVIATIONS

A – absorption

AAS – atomic absorption spectroscopy

a.u. – arbitrary units

B – constant associated with absorption

d – layer thickness

EDS – energy dispersive X-ray spectroscopy

E_g – band gap energy

hv – photon energy

k_t – rate constant

SEM – scanning electron microscopy

UV/VIS – ultraviolet–visible spectroscopy

XPS – X-ray photoelectron spectroscopy

XRD – X-ray powder diffraction

α – absorption coefficient

λ – wavelength

INTRODUCTION

Global climate change and greenhouse gas emissions are widely recognized problems. Developed countries are looking for ways to deliver electricity which would be carbon neutral, environmentally friendly and renewable. Another reason why the development of renewable energy resources in Lithuania is important is a need to reduce the country's dependency on imported fuel. The development of renewable energy sources has been growing in recent years. At the moment, the leading options of renewable energy sources are: wind, geothermal, marine and solar.

Solar cells are one of the most prominent and promising energy technologies today. It is sustainable, renewable, clean, completely noise-free, scalable, requires minimal amount of maintenance and produces zero emissions. Moreover, energy obtained using solar cells is easy to distribute and allows to skip expensive grid infrastructure. The sun is considered as the most abundant source of energy in existence.

The formation of semi-conductive chalcogenide layers on different substrates has been intensively studied over the last years. The development of new materials and optimization properties of the known selenide precursors, including selenopolythionates, are of great importance to obtaining layers with the optimal properties.

The ternary compound (I–III–VI_2) semi-conductor $CuInSe_2$ is one of the leading materials for large-scale solar applications. It has a direct band gap, a high absorption coefficient, stability against photodegradation and good thermal stability. Copper selenide is a semi-conducting material, which exhibits electrical and optical properties suitable for photovoltaic application.

This thesis is related to the search of new effective methods to obtain copper and indium selenide layers. Copper and indium selenide layers were obtained on glass using a low cost, simple successive ionic layer adsorption and reaction (SILAR) method. This method produces homogeneous layers and allows for easy scalability for large surface area coatings.

Aim of the work

The aim of this work is to study the $H_2Se_nS_2O_6$ type selenopolythionate acids as a selenization agent and obtain copper and indium selenide layers on glass.

To achieve our task, the following objectives were formed:

1. To synthesize and study the $H_2Se_nS_2O_6$ type selenopolythionate acids.
2. To obtain selenium, copper selenide, copper and indium selenide layers on glass using selenopolythionate acids.
3. Using various analysis methods, to study the physical and chemical composition, morphology and optical properties of the obtained layers.
4. To study and determine the formation mechanisms of copper and indium selenide layers.

Scientific novelty

This research has shown for the first time that it is possible to obtain selenium layers on glass using the $H_2Se_nS_2O_6$ type selenopolythionate acids. Using selenopolythionate acids as a selenization agent and a simple SILAR method, copper and indium selenide layers were obtained. Layers were described using XRD, XPS, SEM/EDS and AAS methods. The optical properties of the aforementioned layers were determined.

Approval and publication of research results

Results of the research were presented in 6 publications: 2 of them were presented in journals listed in the *Thomson Reuters™ Web of Science* publication database; 4 articles were reported in the proceedings of conferences.

Structure and content of the dissertation

The dissertation consists of an introduction, a literature review, the experimental part, results and discussion, conclusions, a list of references, a list of publications and proceedings on the topic of the dissertation. The list of references includes 161 bibliographic sources. The results are discussed in 81 pages, illustrated in 11 tables and 23 figures.

Statements presented for the defence:

1. $H_2Se_nS_2O_6$ type selenopolythionate acids can be synthesized directly.
2. This type of selenopolythionate acids can be used as a precursor for selenium layer deposition on glass.
3. Copper and indium selenide layers can be obtained using a three-step method.
4. The successive ionic layer adsorption and reaction (SILAR) method is suitable for the formation of metal selenide layers.

1. LITERATURE REVIEW

1.1. Copper selenide

1.1.1. Copper selenide properties

Copper selenide is a binary metal chalcogenide consisting of copper and selenium. Its formula is typically described as CuSe or Cu_2Se, but it is non-stoichiometric. The known stoichiometries are: Cu_2Se, Cu_3Se_2, Cu_5Se_4, CuSe, $CuSe_2$ and the intermediate $Cu_{2-x}Se$ and $Cu_{4-x}Se_2$ [1].

Cu_2Se forms a cubic C1-type lattice with the 4 copper atoms located on the cube's corners and the centres of the cube's sides; selenium atoms lay on diagonals of all directions at ¼ of the distance from the cube's edges [2]. Cu_2Se, just as all other compounds with same cubic C1 lattice, have a fixed melting temperature and a defined chemical formula. Selenium atoms form a rigid framework of the crystal lattice, while Cu ions are distributed on different interstitial sites [3].

Heated or electrochemically polarized orthorhombic copper(I) selenide changes its phase to cubic [4]. The thermal stability of CuSe depends on their stoichiometry. It is also know that high temperature $Cu_{2-x}Se$ (x = 0.18–0.25) cubic and low temperature monoclinic/orthorhombic modifications exist [5]. The high temperature cubic modification is more stable at 75°C and above [6]. $Cu_{2-x}Se$ is diamagnetic at 93°C and above [7, 8]. $Cu_{2-x}Se$ is less stable in normal conditions than Cu_2Se_3 [8]. The structure of cubic copper selenide $Cu_{2-x}Se$ is matched by stoichiometric compound $Cu_{1.96}Se$.

$Cu_{2-x}Se$ is reported to possess a direct band gap of 2.2 eV and an indirect band gap of 1.4 eV, when x = 0.2 [9]. The direct band gap is preferred over the indirect one, due to its fast response and reasons of momentum conservation. The optical and electrical properties of these films depend on the fabrication method chosen after considering the variety of compositional complexity of copper selenides. Moreover, the possible phase transitions greatly depend on the x value [10]. In vacuum evaporated thin films of $Cu_{2-x}Se$, the hole mobility is of the order of 10 $cm^2\ V^{-1}\ s^{-1}$ and carrier concentrations are in the range of 10^{18}–10^{21} cm^{-3}, when the x values are between 0.1 and 0.3 [9].

1.1.2. Copper selenide application

Copper chalcogenide thin films have a number of applications in various devices, such as solar cells, photodetectors, superionic conductors, photoconductors, sensors, photothermal conversion, electro-conductive electrodes, narrow band filters, microwave shielding coating, flexible thermoelectric units, etc. [11–14]. Copper selenide is a semiconducting material which has electrical and optical properties suitable for photovoltaic application. All copper selenides are p-type semi-conductors,

and their holes originate from the Cu deficiency [15]. This property is useful for solar cell production.

Copper selenide is produced directly on iron or steel parts to form a protective black coating in some cold-bluing processes for protection against rust. Bluing solutions which operate in this manner are typically labelled as containing selenous acid or selenium dioxide [16].

$CuSe_2$ nanoneedles are grown on copper foil as a binder-free electrodes to be used as supercapacitors or electrochemical capacitors [17]. It has also been investigated for treating colon cancer [18]

1.1.3. Copper selenide formation methods

Copper selenide is frequently grown as nanoparticles or other nanostructures. It can be obtained by using various chemical and physical methods:

1) Direct elemental reaction is conducted without air at 200–400°C. $Cu_{2-x}Se$, Cu_3Se_2, CuSe, and $CuSe_2$ are obtained by melting equivalent amounts of elemental copper and selenium in slightly higher than melting temperature [19].
2) Hydrogen selenide reaction with simple copper compounds. Copper (II) oxides and salts react with a gaseous or H_2Se water solution:
$$CuSO_4 + H_2Se \leftrightarrow CuSe + H_2SO_4 \quad (1)$$
$$CuCl_2 + H_2Se \leftrightarrow CuSe + 2HCl \quad (2)$$
Nonstoichiometric copper selenide compounds are formed in $CuCl_2$ and H_2Se solutions in different pressures and temperatures. Berzelianite $Cu_{2-x}Se$ is formed in high pressure, while umangite Cu_3Se_2 is formed in lower pressure [20].
3) Selenium vapour reaction with simple compounds. Crystalline Cu_2Se is formed by elemental copper and selenium vapour reaction [21]:
$$2Cu + Se \rightarrow Cu_2Se \quad (3)$$
4) Various copper salts reduction using hydrogen, ammonia, carbon, or hydrazine [20, 21]:
$$CuSeO_4 + 4H_2 \rightarrow CuSe + 4H_2O \quad (4)$$
$$2CuSeO_3 + 3N_2H_4 \rightarrow 2CuSe + 3N_2 + 6H_2O \quad (5)$$
5) Higher selenide thermal decomposition [20]:
$$2MSe_2 \rightarrow M_2Se_3 + Se \quad (6)$$
6) Treating elemental selenium with copper (I) salt solutions. CuSe is formed by treating $CuCl_2 \cdot 2H_2O$ with elemental selenium in a diluted ammonia solution [22], while $Cu_{2-x}Se$ is obtained by treating copper (I) chloride with sodium oxalate [23].
7) Electrodeposition method is based on the electrolysis of certain solutions, i.e. sodium thiosulfate, when elemental selenium is the cathode and copper

is the anode. Using acidic $CuSO_4$ and SeO_2 solutions, layers of Cu_2Se can be deposited [24]. Cu_2Se, Cu_3Se_2, CuSe and their mixtures can be deposited using Cu(II) and Se(IV) solutions in citric acid [25].

8) Chemical deposition. N,N-Dimethylselenourea [26] or selenosulfate [27, 28] can be used as a source of selenium to obtain CuSe or $Cu_{2-x}Se$ [29–31].
9) Using the sonochemical method. Phases of Cu_3Se_2, $Cu_{2-x}Se$, and CuSe can be obtained using this method. Different phases can be obtained by changing the Cu^{2+} / $SeSO_3^{2-}$ ion concentration in the precursor solution and by changing the irradiation time [32–35].
10) Nonstoichiometric $Cu_{2-x}Se$ compounds can be formed at room temperature using gamma rays [36], visible light [37] or microwave radiation [38].
11) CuSe can be reduced into Cu_2Se, and vice versa, Cu_2Se can be oxidized to CuSe [39].

Copper selenides can be oxidized using nitric acid and aqua regia [12].

$$3Cu_2Se + 22HNO_3 \rightarrow 6Cu(NO_3)_2 + 3H_2SeO_4 + 10NO + 8H_2O \quad (7)$$

Cu_2Se oxidizes in two stages in a base medium. The reaction is rapid only at 200°C [2]:

$$Cu_2Se + 2O_2 + 2HO^- \rightarrow 2CuO + SeO_3^{2-} + H_2O \quad (8)$$

$$2SeO_3^{2-} + O_2 \rightarrow 2SeO_4^{2-} \quad (8)$$

Similarly, Cu_2Se oxidizes in two stages in an acidic medium [2]:

$$2Cu_2Se + O_2 + 2H_2SO_4 \rightarrow 2CuSe + 2CuSO_4 + 2H_2O \quad (9)$$

$$2CuSe + O_2 + 2H_2SO_4 \rightarrow 2Se + 2CuSO_4 + 2H_2O \quad (10)$$

1.1.4. Copper selenide minerals

Copper selenide is found in nature in various stoichiometries as various minerals.

Berzelianite is a rare mineral with the formula $Cu_{2-x}Se$. It occurs as thin dendritic crusts or as fine-grained inclusions. Berzelianite crystallizes in the isometric system, unlike its dimorph, bellidoite, which crystallizes in the tetragonal system. The crystals of berzelianite are opaque and slightly malleable.

Bellidoite is a tetragonal-dipyramidal silver grey mineral with the stoichiometric formula of Cu_2Se. It is of creamy white, greyish colour. Bellidoite is formed at medium to low temperatures with other hydrothermal selenides and sulphides.

CuSe can be found as a mineral klockmannite. Klockmannite displays low temperature modification at less than 50°C, and high temperature modification at 50°C and above. It decomposes into $Cu_{2-x}Se$ and Se at 379°C [40, 41]. It was determined that in low temperature CuSe has the same structure as CuS mineral

covellite. In a high pressure of 52 GPa, the S–S bond becomes shorter, while the Se–Se does not [42].

Cu_3Se_2 is found in nature as a mineral umangite. It was determined that Cu_3Se_2 decomposes to $Cu_{2-x}Se$ and CuSe below 170°C [8]. Cu_3Se_2 occurs only in small grains or fine granular aggregates with other copper minerals of the sulphide group. Its colour ranges from blue-black to red-violet with a black streak.

Krut'aite is a rare mineral with the formula of $CuSe_2$. It crystallizes in the cubic system. The mineral is often found as a dark grey aggregate, consisting of smaller than one millimetre size crystals.

Copper selenide Cu_5Se_4 is found in the form of athabascaite mineral, which forms with other copper selenides. There is little known about the atomic structure of athabascaite because sufficiently large single crystals are unavailable. The symmetry of the crystal appears to be orthorhombic. It has a calculated density identical to that of umangite, therefore it is thought to have a similar structure [43]. The colour of athabascaite is typically light grey; however it can also be white, blue-grey or white-grey. Athabascaite displays a range of colours varying from creamy white to dark blue when exposed to polarized light. Its reflectivity along with these distinct colours, allows athabascaite to be easily distinguished from other copper selenide minerals [44].

All minerals which can be found in nature and contain copper selenide are shown in the Table 1.

Table 1. Minerals containing copper selenide

Name	Athabascaite [45]	Bellidoite [46]	Berzelianite [47]	Klockmannite [48]	Krut'aite [49]	Umangite [50]
Formula	Cu_5Se_4	Cu_2Se	$Cu_{2-x}Se$ (Cu_2Se)	CuSe	$CuSe_2$	Cu_3Se_2
Molecular weight, g/mol	633.57	206.05	206.05	142.51	221.47	348.56
Composition	Cu 50.15 % Se 49.85 %	Cu 61.68 % Se 38.32 %	Cu 61.68 % Se 38.32 %	Cu 44.59 % Se 55.41 %	Cu 28.69 % Se 71.31 %	Cu 54.69 % Se 45.31 %
Synonym	IMA1969-022	ICSD 30230, PDF 46-1129	ICSD 238, PDF 6-680	ICSD 82331, PDF 34-171	ICSD 243, PDF 26-1115	ICSD 239 PDF 47-1745
System	Orthorhombic	Tetragonal - Dipyramidal	Isometric - Hexoctahedral	Hexagonal - Dihexagonal Dipyramidal	Isometric - Diploidal	Orthorhombic - Disphenoidal
Environment	As inclusions and replacements of umangite.	Formed at moderate to low temperature with other hydrothermal selenides and sulphides.	Forms with other selenides in hydrotherma veinlets in dolomite.	Of hydrothermal origin.	Of hydrothermal origin included in clausthalite.	Found with other selenides in hydrothermal veins.
Growth habits	Anhedral Grains, Microscopic Crystals	-	Dendritic, Disseminated, Massive	Aggregates, Granular	Inclusions	Uneven, Massive, Granular
Hardness	2.5–3	1.5-2	2	2-2.5	4	3
Colour	Blue grey, Grey white	Silver grey	Bluish grey, Grey, Black	Blue black, Greyish black, Dark grey	Grey	Blue black, Brownish black, Red violet
Luster	Metallic	Metallic	Metallic	Metallic, Dull	Metallic	Metallic
Diaphaneity	Opaque	Opaque	Opaque	Opaque	Opaque	Opaque
Density	6.63	7.03	6.7	5.99	6.62	6.2
Space group	-	P 4_1/m	F m3m	P 6_3/mmc	P a3	P 2_12_12
a	8.227	11.52	5.739	3.938	6.056	6.4
b	11.982	-	-	-	-	12.46
c	6.441	-	-	17.25	-	4.28
Z	4	32	4	-	4	4
V	634.93	1558.02	189.02	-	222.10	341.30

1.2. Indium selenide

1.2.1. Indium selenide properties

Indium selenide has a number complicated stoichiometries, including the forms of InSe, In_2Se_3, In_4Se_3, and In_6Se_7 [51]. Like most of the III–VI compounds, In_2Se_3 has a tetrahedral bonding structure [51]. Indium selenide (In_3Se_2) is a III–VI semi-conductor with a direct optical band gap of a value in the range of 1.4–1.7 eV [52, 53]. It is capable of absorbing most of the visible light spectrum of the solar radiation in its nano particle form [54]. In layered compounds like In_2Se_3 or InSe a primitive layer is formed, which consists of four atomic planes, Se–In–In–Se. The selenium atoms form two-dimensional hexagonally close-packed sheets, while giving these crystals their hexagonal structure. The atoms are aligned along the c axis in every other trigonal prismatic structure [52]. The cation vacancies form a plane, which results in weak Se–Se bonding and anisotropic electronic properties. In_2Se_3 and InSe also tend to have high resistivity [55]. In_4Se_3, on the other hand, is a highly conductive smaller-band gap orthorhombic semi-conductor [56]. The higher conductivity of In_4Se_3 is attributed to the presence of In–In bonds, while in the other In–Se compounds indium bonds only to selenium [57].

1.2.2. The application of indium selenide

Out of the many available semiconductors, metal chalcogenides in the III–VI group of layered semi-conductors are assumed to have applications of great importance, in various optoelectronic devices, including photovoltaic. This is due to their narrow and tunable optical band gaps. Due to its optical properties, In_2Se_3 has emerged as a potential candidate, mostly in solar cell applications, nanoscale optical, electrical, and optoelectronic devices. The In_2Se_3 films have also been studied as a precursor to $CuInSe_2$ for solar cell application [58].

1.2.3. Indium selenide deposition methods

There are many methods reported in literature which are available for the synthesis of In_2Se_3 using various techniques showing three different phases α, β and γ [59, 60] with a range of morphologies [61, 62] including thin films [63] and nano-materials [64]. Amongst various deposition methods, the sol–gel technique is the least expensive and simplest method that could be used to produce thin films in large areas. There are two main challenges regarding the formation of indium selenide films. First, the hydrolyzation of In (III) cations is in an aqueous solution due to their deficient electron properties, which effects the formation of indium selenide [65]. Second, indium selenide has a lot of complicated stoichiometries [51].

1.3. Copper indium selenide

1.3.1. Copper indium selenide properties

$CuInSe_2$ belongs to the group of ternary chalcopyrite compounds which derive from group IV of tetrahedrally bonded semi-conductors. There must be an average of 4 valence atoms per atomic site. In these structures, each atom has four neighbouring ones arranged at the corners of a regular tetrahedron bonded with sp^3 bonds. The tetrahedral structure of a chalcopyrite has a diamond-like structure consisting of two inter-penetrating face-centred cubic lattices [66].

In a ternary chalcopyrite, the cations are replaced by one cation of higher valency (In) and 13 cations of lower valency (Cu) which occupy the cation sub-lattice in an ordered manner, as shown in Fig. 1.

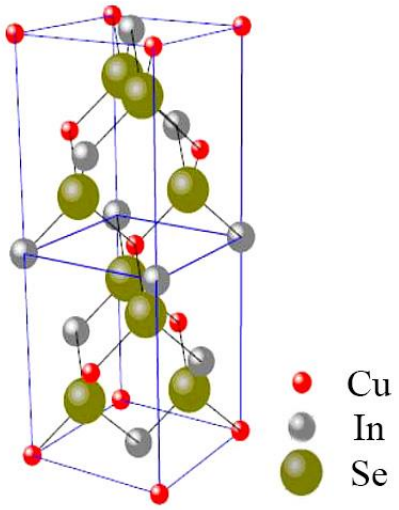

Fig. 1. The structure of copper indium selenide molecule [67]

Copper indium selenide can be obtained under n or p-type conductivity [68]. The direct band gap energy is at the red edge of the solar spectrum, which corresponds with the high optical absorption coefficient ($>10^5$ cm^{-1}) [69]. 1 μm thick layer of $CuInSe_2$ absorbs 90% of solar irradiation that has higher energy than its corresponding band gap (1.04 eV) [70]. $CuInSe_2$ has high thermal stability [71] which does not degrade its performance under intense, high-energy solar irradiation [72]. It also has a large calculated exciton Bohr radius of ~10.6 nm. The bulk copper indium selenide material shows excellent photovoltaic performance [73].

Some copper indium selenide properties are shown in Table 2.

Table 2. The physical properties of $CuInSe_2$ [74]

Property	Value	Unit
Formula	$CuInSe_2$	
Molecular mass	336.28	g mol^{-1}
Density	5.77	g cm^{-3}
Colour	Grey	
Transition to sphalerite structure	810	°C
Melting temperature	986	°C
Symmetry	Chalcopyrite	
Space group	$I42d–D^{12}_{2d}$	
Lattice parameters		
a_0	0.5789	nm
c_0	1.162	nm
Thermal expansion coefficient (at 273 K)		
a axis	$8.32 \cdot 10^{-6}$	K^{-1}
c axis	$7.88 \cdot 10^{-6}$	K^{-1}
Thermal conductivity	0.086	W cm^{-2} K^{-1}
Specific heat		
c_1	$–7.67 \cdot 10^{-4}$	K^{-1}
c_2	$4.06 \cdot 10^{-6}$	K^{-2}
c_3	$4.3 \cdot 10^{-9}$	K^{-3}
Debye temperature	221.9	K
Micro hardness	$3.2 \cdot 10^{-9}$	N m^{-2}
Compressibility	$1.4 \cdot 10^{-11}$	m^{-2} N
Dielectric constant		
Low frequency	13.6±2.4	
High frequency	8.1±1.4	
Sound velocity	$2.2 \cdot 10^2$	m s^{-1}
Electrical resistivity (polycrystalline thin films)		
Cu-rich	0.001	Ω
In-rich	>100	Ω
Mobility (300 K)		
Electrons	100–1000	cm^2 V^{-1} s^{-1}
Holes	50–180	cm^2 V^{-1} s^{-1}
Effective mass		
Electrons	$8.20 \cdot 10^{-32}$	kg
Holes	$8.38–64.68 \cdot 10^{-32}$	kg
Band gap	1.04	eV
Temperature dependence of gap dE_g/dT (77–300 K)	$–2 \pm 10^{-4}$	eV K^{-1}
Pressure dependence of gap dE_g/dP	$–2.8 \pm 10^{-11}$	eV Pa^{-1}

1.3.2. The application of copper indium selenide

Copper indium selenide is widely investigated as an absorber layer material in thin film solar cell applications and has attracted considerable attention due to its desirable physical properties. It is best known as the material for thin-film technology used in the photovoltaic industry. It has the advantage of being formed on various substrate materials, producing highly flexible and lightweight solar panels. Constant improvements in efficiency have made $CuInSe_2$ an established technology among other alternative cell materials. Copper indium selenide and other chalcopyrite family of materials is relevant in many fields, including nonlinear optics, optoelectronic, and photovoltaic devices [66].

1.3.3. Copper indium selenide deposition methods

Thin copper indium selenide layers can be obtained either through chemical or through physical deposition. Chemical deposition methods offer low cost production of homogeneous layers and easy scalability for large surface area coatings. However, annealing is required to obtain crystalline $CuInSe_2$ layers.

Physical deposition, on the other hand, offers layers with better properties, while often requiring high cost low-pressure, high-temperature equipment. Furthermore, it does not offer good scalability for large-area coating. Also, physical deposition techniques often require annealing in Se or H_2Se atmosphere, which results in reagent wastage, toxic work environment and even lower cost efficiency. Both chemical and physical deposition methods can be divided further.

Chemical deposition methods:

Chemical bath deposition method is using substrate submerged into a precursor solution. This method is also known as the *sol-gel* method because the precursor solution gradually evolves towards a two-phase gel-like system. It offers several advantages, such as the possibility to cover both large and small areas, reliability, and easily replicable results. This method uses very simple and cheap equipment and creates a non-toxic work environment. Usually two baths are used as precursors $CuSO_4$, $In_2(SO_4)_3$ and Na_2SeSO_3 [75–77].

Electrodeposition is when a metal film is deposited from an ionic solution using an electric current. CuInSe2 layers are obtained from aqueous solutions using an electric current. This system consists of one or more electrolytes, a cathode and an anode. The obtained properties depend on the solution's temperature and concentration [78], pH [79], deposition duration as well as the used electrolyte additives, such as complexing agents [71]. Similarly, to CBD and other non-vacuum processes, electrodeposition offers a number of advantages, for instance, simple equipment, low cost, low temperature operation, the ability to deposit large areas with

ease, fast deposition rates, easily controlled layer thickness, no need for very pure reagents. Another advantage of electro deposition is that this method is "green" and does not require the use of toxic reagents, such as H_2Se gas or Se vapour. One of the disadvantages of this deposition method is that the deposited layers are often amorphous and require annealing at 500–600°C to obtain high quality crystalline layers and increase grain size [80]. The annealing must be performed in Se atmosphere to prevent loss from the layer [81]. In addition, completely aqueous solutions introduce the formation of insoluble and non-conductive metal hydroxides at the cathode. Organic, non-aqueous, usually toxic solutions can be used to overcome this. Using organic solvents, more negative voltages can be applied and higher operating temperature can be obtained [80]. Also, it is important that Cu^0 deposits faster than In^0 due to different Cu^{2+}/Cu and In^{3+}/In redox potentials. This tends to form undesired $Cu_{2-x}Se$ that worsens the properties of the layer. The electrodeposition method has been successfully used for the deposition of elemental, binary, ternary and quaternary compounds [82]. Various additives can be used to minimize the formation of $Cu_{2-x}Se$ [75, 83, 84]. Electrodeposition can consist of one or two steps. One-step electro deposition is performed when all required components are deposited directly on a substrate from a single solution. This produces the best quality large-area layers of $CuInSe_2$ [71, 85]. Two-step deposition involves obtaining the Cu–In layer first, then In–Se, or Cu–Se, and finally, In–Se [86].

Physical deposition methods:

Chemical vapor deposition (CVD). This process involves a wafer (substrate) which is exposed to more volatile precursors which react and decompose on the surface of the substrate. The biggest challenge of using this method is finding volatile Cu and In precursors. Metal-organic compounds can be used to increase precursor volatility; metals with organic ligands are dissolved in organic compounds. This deposition method is called *metal organic chemical vapor deposition (MOCVD)*. It offers several advantages; it is rather easy to obtain high quality layers with less impurities and uniform thickness [87]. Also, the stoichiometric ratio of used elements is relatively easily controlled [88]. The success of the MOCVD process depends on highly volatile and thermally stable precursors. These thermal properties are important to achieve uniform thickness and reproducible layers [89]. The drawbacks of this method include high temperatures of the process, high cost, and low pressure.

Chemical spray pyrolysis (CSP) is a thin-film deposition technique which involves spraying a metal-salt solution onto a heated substrate. Droplets which impact on the surface of the substrate undergo thermal decomposition and form a thin layer. Among the various deposition techniques, spray pyrolysis is the most convenient method for water-soluble salts. It is a very simple and relatively cost-effective method,

especially regarding the equipment cost; it also does not require high quality substrates or chemicals. Even multi-layered films can be easily prepared using this technique. This simple and inexpensive experimental arrangement provides the ease of adding doping materials, a high growth rate and the ability to mass-produce uniform large-area coatings [90, 91].

Spin coating uses liquid or sol-gel precursors, often Cu_2Se and In_2Se_3 dissolved in organic compounds, to deposit onto a smooth, flat substrate which is spun at a high velocity to spread the solution over the glass substrate. The factors that determine the thickness of the deposited film are speed at which the solution is spun and the viscosity of the solution [92]. Repeated depositions can be carried out to increase the thickness of the layer. Often, thermal treatment is carried out at 350°C in inert N_2 or Ar atmosphere in order to crystallize the amorphous coated layer [92]. Such crystalline layers can exhibit certain preferred orientations after crystallization on single crystal substrates [93]. Depending on weather the used precursors contain Se, a post-process selenization may be needed [94] or not [92]. Spin coating is not a vacuum process, thus, similarly to other non-vacuum processes, it does not require complicated, costly, low pressure equipment.

Physical vapor deposition (PVD) involves evaporating the precursor material and escaping particles towards cooler substrate, which draws energy from them to form a thin film. The whole system is kept in a vacuum deposition chamber, allowing particles to travel freely. This reduces the incorporation of impurities from the residual gas in the vacuum chamber. While the PVD method produces high quality layers, it requires expensive, complex, low-pressure equipment to ensure sterile deposition environment. Hence, the used precursor materials must be really pure in order to get pure layers. Also, this method is hard to scale for large-area layer deposition. Another big drawback is that this method includes a post-selenization process at 450–600°C under H_2Se or Se vapor atmosphere [95]. This introduces a toxic work environment, high reagent wastage and pollution. All these drawbacks make PVD a very expensive deposition procedure, depending on the technique used to evaporate the substrate.

Thermal evaporator uses an electric resistance heater to melt the substrate material and raise its vapor pressure. Only materials with higher vapor pressure than the heating element can be deposited without contamination. For economic reasons and simplicity, low-cost deposition methods are actively studied. Thermal evaporation of the synthesized $CuInSe_2$ powder is the simplest method. However, the dissociation of the ternary compound into binary ones as the source temperature is increased may result in selenium-deficient and non-stoichiometric films [96]. To overcome these drawbacks, *flash evaporation (a.k.a. rapid thermal processing)* method can be employed. This method includes a fine wire of the source material fed continuously onto a hot ceramic bar and being evaporated on contact. Flash-evaporated $CuInSe_2$

thin films under selenium environment result in single-phase, stoichiometric $CuInSe_2$ thin films at substrate temperature as low as 350°C [97]. *Co-evaporation* is a complex processing technique which includes two material sources being evaporated at the same time or sequentially. It requires accurate temperature control over the individual precursors to ensure and uniform fluxes as well as a high degree of stoichiometric uniformity [98].

Sputtering. Noble inert gases, usually argon, are used to knock out a few atoms at a time from Cu_2Se and In_3Se_2 targets. Because the process does not include evaporation, the target can be kept at a low temperature, making this the most versatile deposition method. One of the advantages of this method is fast layer formation and relatively easy thickness control. It is also very useful for compounds of mixtures with different compounds that evaporate at different rates. *Radio frequency (RF) sputtering* process has the advantages of admirable stoichiometry transfer of the target material and large-area uniformity. Disadvantages include poor adhesion at back contact and poor reproducibility [95, 99].

Molecular beam epitaxy uses guns, called effusion cells, to fire relatively precise beams of molecules (heated in gas form) at the substrate. This is one of the most expensive and slow processes, which also requires ultra-high vacuum. Multiple "guns" are needed for each beam of molecules. The molecules land on the surface of the substrate, condense, and build up ultra-thin layers, therefore, the single crystal grows one atomic layer at a time [100–102].

1.4. Selenium precursor properties

1.4.1. Methods of selenopolythionates synthesis

Anions of selenopolythionates can be considered as the substituted polythionates in which sulphur is partially replaced by selenium. As a result, more different forms of anions appear: the following homologous ranges are known now $Se_nS_2O_6^{2-}$(n = 1 – 6), $Se_nS_3O_6^{2-}$(n = 1 – 3), and $SeS_nO_6^{2-}$(n = 2 – 4).

Comparative studies of the homologous range $Se_nS_2O_6^{2-}$(n = 1 – 6) when the composition of anion is variable and an investigation of the properties of individual members are mutually complementary.

The first representative of this group is selenotrithionate acid $H_2SeS_2O_6$, that was discovered and obtained as potassium salt $K_2Se(SO_3)_2$ by Rathke in 1865 [103]. He treated selenous acid with concentrated disulphite. Foerster and co-authors suggested this reaction mechanism [104]:

$$SeO_2 + 4H^+ + 4SeSO_3^{2-} \rightarrow Se_2S_2O_6^{2-} + Se(SeSO_3)_2^{2-} + 2H_2O \quad (11)$$

$$Se(SeSO_3)_2^{2-} + SO_3^{2-} \rightarrow Se_2S_2O_6^{2-} + SeSO_3^{2-} \quad (12)$$

$$Se_2S_2O_6^{2-} + SO_3^{2-} \rightarrow SeS_2O_6^{2-} + SeSO_3^{2-} \quad (13)$$

The summing equation is:

$$SeO_2 + 4H^+ + SeSO_3^{2-} + 3SO_3^{2-} \rightarrow 2SeS_2O_6^{2-} + 2H_2O \quad (14)$$

This meant that in case of disulphite excess, selenotrithionate is the only reaction product. The yields of this synthesis method is about 80%.

Other synthesis methods were also discovered. Most of them, similarly to Rathke's method, were based on the oxidation of selenosulfate ions, i.e. iodine, hydrogen peroxide [105], or using electrolysis [106]:

$$2SeSO_3^{2-} + 2e^- \rightarrow Se_2S_2O_6^{2-} \quad (15)$$

Later, selenosulfate was obtained by degrading the intermediate product, diselenotetrathionate using sulphite.

Selenous acid reduction using sulphurous acid is also rather well-known [107]:

$$H_2SeO_3 + 2H_2SO_3 \rightarrow 2H_2SO_4 + Se + H_2O \quad (16)$$

It is widely used for making elemental selenium. This reaction is complicated and intermediate products $Se_nS_2O_6^{2-}$ are formed. Schulze noticed that selenous acid in excess of sulphurous acid form selenotrithionate acid [108]:

$$H_2SeO_3 + 3H_2SO_3 \rightarrow H_2SO_4 + H_2SeS_2O_6 + 2H_2O \quad (17)$$

Quantitatively, this reaction was studied in [109]. It was discovered that while pouring sulphurous acid to an excess of selenous acid, diselenotetrathionate acid is formed:

$$2H_2SeO_3 + 5H_2SO_3 \rightarrow H_2Se_2S_2O_6 + 3H_2SO_4 + 3H_2O \quad (18)$$

Free acid substitution with potassium hydrosulphite enables the use of higher concentration solutions and allows obtaining of crystalline $K_2Se_2S_2O_6 \cdot H_2O$ [110].

Moreover, lithium, sodium, potassium, rubidium, cesium and other metal selenotrithionates were obtained in crystal form [111]. J. Janickis and V. Zelionkaite isolated the first salt of diselenotetrathionate acid, the monohydrate $K_2Se_2(SO_3)_2\ H_2O$ [105].

However, unsolved acids had not been prepared until quite recently: Zelionkaite and Šukytė in 1970–1972 synthesized the solvent-free selenotrithionate $H_2SeS_2O_6$, and diselenotetrathionate $H_2Se_2S_2O_6$ acids [112]. These acids were isolated from their potassium salts. Potassium selenotrithionate and diselenotetrathionate were synthesized according to the published procedures [111, 113]. Anions of ranges $Se_nS_2O_6^{2-}$(n = 1 – 6) and $Se_nS_3O_6^{2-}$(n = 1 – 3) were isolated only in the form of nitrone salts and some complex cobalt cations [105].

Austad discovered that elemental selenium reacts with acetonitrile and forms diselenotetrathionate, unlike in a water solution [114]:

$$(x+2)Se + 2SO_3^{2-} \rightarrow Se_2S_2O_6^{2-} + Se_x^{2-} \quad (19)$$

Using this reaction, tetraphenylarsonium diselenotetrathionate $[(C_6H_5)_4As]_2Se_2S_2O_6$ was synthesized with about 60% yield.

Norris and Fay discovered that selenous acid oxidizes thiosulfate in acidic medium [115]:

$$SeO_2 + 4Na_2S_2O_3 + 4HCl \rightarrow Na_2SeS_4O_6 + Na_2S_4O_6 + 4NaCl + 2H_2O \quad (20)$$

This reaction can be used to quantitatively measure selenous acid and selenites. Heuer confirmed this reaction and extracted crystalline potassium diselenotetrathionate from a mixture of products [116].

In 1949 Foss synthesized crystalline sodium and potassium selenopentathionate, and later rubidium, cesium, ammonia [117] and barium salts [118].

Firstly, asymmetric selenopolythionate – monoselenotetrathyonate $^{-}O_3S–Se–S_2O_3^{-}$ salts were obtained using a complex cobalt (III) cation. Selenotrithionate was treated with thiosulphate 1:1 molar ratio [119, 120]:

$$SeS_2O_6^{2-} + S_2O_3^{2-} \rightarrow SeS_3O_6^{2-} + SO_3^{2-} \quad (21)$$

Soon monoselenotetrathionate was synthesized by treating selenotrithionate with selenopentathionate [121, 122]:

$$SeS_2O_6^{2-} + SeS_4O_6^{2-} \rightarrow 2SeS_3O_6^{2-} \quad (22)$$

The reaction results in potassium monoselenotetrathionate salt $K_2SeS_3O_6 \cdot H_2O$, that is well soluble in water.

1.4.2. The properties of selenopolythionates

Selenopolythionates have similar properties to regular polythionates, but are less stable. The more there are Se atoms in the molecule, the less stable they are. Additionally, the type and speed of decomposition depends on the pH of the aqueous solution, its concentration, temperature and exposure to solar irradiation [123]. Decomposition in acidic solution can be represented as:

$$SeS_2O_6^{2-} + HOH \rightarrow Se + SO_4^{2-} + H_2SO_3 \quad (23)$$

This reaction mechanism is explained through selenotrithionate hydrolysis:

$$Se(SO_3)_2^{2-} + HO\text{H} \rightarrow HSeSO_3^- + HSO_4^- \quad (24)$$

Then, selenosulfate reacts with selenotrithionate that did not decompose:

$$Se(SO_3)_2^{2-} + HSeSO_3^- \rightarrow Se_2(SO_3)_2^{2-} + HSO_3^- \quad (25)$$

And after most of $SeS_2O_6^{2-}$ decomposes, selenosulfate which is not stable in an acidic medium decomposes:

$$SeSO_3^{2-} + H^+ \rightarrow Se + HSO_3^- \quad (26)$$

Then, diselenotetrathionate degrades under the influence of newly formed sulphite:

$$Se_2S_2O_6^{2-} + SO_3^{2-} \rightarrow SeS_2O_6^{2-} + SeSO_3^{2-} \quad (27)$$

Diselenotetrathionate is stable in a mildly acidic solution, but decomposes promptly in highly acidic solutions [109]:

$$Se_2S_2O_6^{2-} + H_2O \rightarrow 2Se + SO_4^{2-} + H_2SO_3 \quad (28)$$

Further selenotrithionate and diselenotetrathionate acid studies show that most of selenium is deposited only when the majority of selenotrithionate acid converts to diselenotetrathionate acid [112]:

$$2H_2SeS_2O_6 + H_2O \rightarrow H_2Se_2S_2O_6 + H_2SO_3 + H_2SO_4 \quad (29)$$

The decomposition proceeds analogously to diselenotetrathionate acid decomposition. The reactions show that both selenotrithionate and diselenotetrathionate converts to each other while undergoing decomposition.

The higher selenopolythionates $Se_nS_2O_6^{2-}$ (n = 3–6) decompose in water or an acidic solution according to this general equation [124]:

$$Se_nS_2O_6^{2-} \rightarrow xSe + Se_{n-x}S_2O_6^{2-} \quad (30)$$

It is analogous to the decomposition of higher polythionate acid $S_nS_2O_6^{2-}$ (n = 2–4) [125]:

$$S_nS_2O_6^{2-} \rightarrow xS + S_{n-x}S_2O_6^{2-} \quad (31)$$

Selenopolythionates $Se_nS_2O_6^{2-}$ (n = 2–4) decompose rapidly in base solutions [124]:

$$2Se_nS_2O_6^{2-} + 6OH^- \rightarrow 2SeSO_3^{2-} + (2n-3)Se + SeO_3^{2-} + 2SO_3^{2-} + 3H_2O \quad (32)$$

Selenotrithionate decomposition is different in these conditions because no elemental selenium is formed; one-mole selenosulfate forms instead of one mole of sulphite [124]:

$$2Se_nS_2O_6^{2-} + 6OH^- \rightarrow SeSO_3^{2-} + SeO_3^{2-} + 3SO_3^{2-} + 3H_2O \quad (33)$$

In a dicarbonate medium, selenopolythionates can be oxidized with iodine to selenite and sulphate ions [124, 125]:

$$Se_nS_2O_6^{2-} + (1+2n)I_2 + (4+6n)OH^- \rightarrow \\ \rightarrow nSeO_3^{2-} + 2SO_4^{2-} + (2+4n)I^- + (2+3n)H_2O \quad (34)$$

In an acidic medium, elemental selenium is formed:

$$Se_nS_2O_6^{2-} + I_2 + 2H_2O \rightarrow nSe + 2HSO_4^- + 2HI \quad (35)$$

Selenopentathionate, unlike other polythionates, is rather stable in an acidic medium. Its slow decomposition can be shown using a general equation [126]:

$$SeS_4O_6^{2-} \xrightarrow{H^+} Se + S_4O_6^{2-} \quad (36)$$

A detailed study shows that the decomposition speed increases with the increasing pH value [127]. This dependency changes when pH > 8. This indicates that the decomposition mechanism in an acidic solution is different from the one in a base solution. When pH is higher (pH=11.0) selenopentathionate decomposes almost instantly:

$$2SeS_4O_6^{2-} + 6OH^- \rightarrow Se + 4S_2O_3^{2-} + SeO_3^{2-} + 3H_2O \quad (37)$$

Selenopentathionate decomposes even faster under sunlight.

Zelionkaitė and Šukytė studied free selenopolythionate acids and synthesized a concentrated 75% selenopentathionate acid by decomposing barium salt using sulphuric acid [127]. They extracted crystalline, yellow, needle-shaped hydrate $H_2SeS_4O_6 \cdot 6H_2O$. They also determined that in the case of concentrated selenopentathionate acid decomposition, sulphuric, sulphurous acids, elemental selenium and sulphur are formed:

$$H_2SeS_4O_6 \rightarrow Se + 2S + SO_2 + H_2SO_4 \quad (38)$$

Monoselenotetrathionate is rather stable in a neutral and mildly acidic medium, however, it less stable than selenotrithionate [128, 129].

Asymmetric $Se_nS_3O_6^{2-}$ type selenopolythionates decompose fast in a strong acidic medium with elemental selenium deposition. Part of the selenium remains in

the solution. It can be removed by adding alkaline to the solution. This is why $Se_nS_3O_6^{2-}$ type selenopolythionates are more resistant to acids than $Se_nS_2O_6^{2-}$ type selenopolythionates which decompose promptly and completely [130] and less resistant than $Se_nS_4O_6^{2-}$ type selenopolythionates which are rather stable in a very acidic medium [124].

Selenopolythionates, just as regular polythionates, degrade under the influence of silver ions, forming black Ag_2Se precipitate. According to Heuer, selenotrithionate decompose under the influence of silver oxide ammonia solution [116]:

$$K_2SeS_2O_6 + Ag_2O \cdot 2NH_3 + H_2O \rightarrow K_2SO_4 + Ag_2Se + (NH_4)_2SO_4 \quad (39)$$

Diselenotetrathionate forms Ag_2Se as well; however, only a small amount, about 5–10% and the remaining selenium is released as elemental selenium [124]. It is also claimed that if the $Se_nS_2O_6^{2-}$ solution is treated with neutral silver nitrate, all selenium is deposited in the form of silver selenide, while the sulphuric acid remains in the solution [128].

$$Se_2S_2O_6^{2-} + 2Ag^+ + 2H_2O \rightarrow Ag_2Se + Se + 2H_2SO_4 \quad (40)$$

1.4.3. The structure of selenopolythionates

The structures of selenotrithionate, diselenotetrathionate, monoselenotetrathionate and monoselenopentathionate ions have been studied extensively.

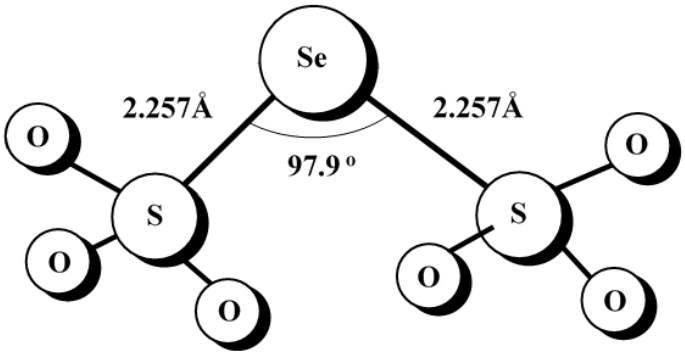

Fig. 2. The structure of selenotrithionate, viewing angle is perpendicular to SeS_2 plain [107]

The analysis of potassium selenotrithionate $SeS_2O_6^{2-}$ showed that the selenium atom is coordinated between two SO_3^{2-} groups (Fig. 2) with a distance of 2,257 Å and an angle of 97.9° [131].

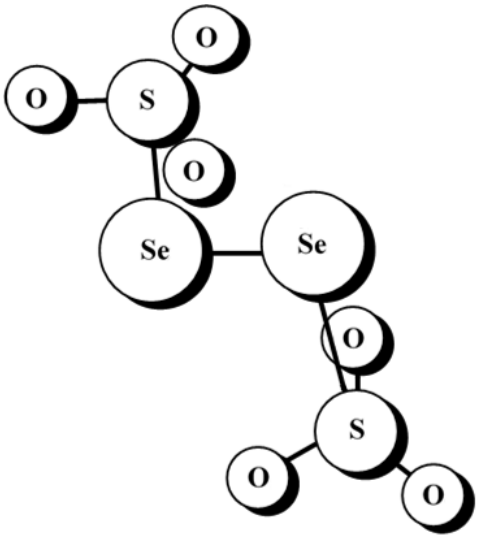

Fig. 3. The structure of diselenotetrathionate ion in crystalline $P2_1/n$ $[Co(en)_2Cl_2]Se_2S_2O_6 \cdot H_2O$ [107]

The structure of diselenotetrathionate ion is studied in $[Co(en)_2Cl_2]Se_2S_2O_6 \cdot H_2O$ modification (Fig. 3) [132]. As we can see, the $Se_2S_2O_6^{2-}$ ion is made of an unbranched and not flat S-Se-Se-S branch.

2. EXPERIMENTAL SETUP

2.1. Selenium precursor analysis

2.1.1. The synthesis of $H_2Se_nS_2O_6$ from selenous acid with the addition of $CaCO_3$

With the aim to precipitate sulphuric acid, an amount of $CaCO_3$ calculated according the following reaction was added:

$$2H_2SeO_3 + 5H_2SO_3 + 3CaCO_3 \rightarrow H_2Se_2S_2O_6 + 3CaSO_4 + 6H_2O + 3CO_2 \quad (41)$$

12 g of $CaCO_3$ was added to 10.4 g of selenous acid dissolved in 10 ml of distilled water,. The mixture was stirred before almost completely removing the CO_2 and forming a suspension of calcium selenite. Then, 150 ml 1.4 mol/l H_2SO_3 was added to the suspension with mixing and cooling it in glass water. At the beginning of the reaction, $H_2SeS_2O_6$ was formed, which further continuously converts to $H_2Se_2S_2O_6$ at room temperature. In order to monitor the reaction, aliquots of solution were taken from the reaction vessel, diluted with distilled water to 100 ml and analysed according to methods described below.

2.1.2. The synthesis of $H_2Se_nS_2O_6$ from selenous acid with the addition of $KHSO_3$

Further, we study the reaction of selenous acid with potassium hydrogen sulphite in more detail:

$$2H_2SeO_3 + 5KHSO_3 \rightarrow H_2Se_2S_2O_6 + 2K_2SO_4 + KHSO_4 + 3H_2O \quad (42)$$

$H_2Se_nS_2O_6$ was prepared using two different preparations with the same mixing molar ratio $2H_2SeO_3$:$5KHSO_3$ by varying only the order of reagent addition to the reaction mixture and the reaction temperature. Both reactions were performed using an excess of one of the reagents, either H_2SeO_3 or $KHSO_3$. In order to monitor the reaction, aliquots of solution were taken from the reaction vessel, diluted with distilled water to 100 ml and analysed according to methods described below.

50 ml of 1 mol/l $KHSO_3$ solution were slowly poured while stirring into the same amount of 0.4 mol/l H_2SeO_3 solution. During reaction, the solution heats up, thus it is cooled down using ice or the solutions must be cooled down beforehand. The solution is greenish-yellowish in colour which indicates the formation of $Se_nS_2O_6^{2-}$ ions. Further, the solution changes colour to orange, then to red with the formation of colloidal amorphous selenium. This solution can be stable for weeks, if refrigerated.

2.1.3. The synthesis of $H_2Se_nS_2O_6$ from $KHSO_3$ with the addition of selenous acid

For the second preparation, the freshly prepared and cooled (1–4°C) 50 ml of 0.4 mol/l H_2SeO_3 was slowly added to the cooled (1–4°C) 50 ml of 1 mol/l $KHSO_3$

with constant stirring. The reaction started spontaneously and was completed within 10 min. The reaction solution is pale green at the beginning, and remains without significant changes for about one month when kept in the refrigerator at 4°C. Further, reaction kinetics was investigated at 25°C using thermostatic arrangement.

2.1.4. Analysis

The complete analysis of the mixture of selenous acid reaction with sulphurous acid with the addition of $CaCO_3$, or selenous acid with potassium hydrogen sulphite includes a determination of the total number of moles of selenopolythionates, the concentration of monoselenotrithionic and diselenotetrathionic acids, the average number of atoms of selenium in a molecule of selenopolythionic acid *n*, the residue of non-reacted selenous acid H_2SeO_3 and also the possible admixtures of the products of its decomposition, namely, elemental Se, sulphurous and sulphuric acids.

Monoselenotrithionic acid oxidizes with iodine in a bicarbonate medium according to the equation:

$$SeS_2O_6^{2-} + 3I_2 + 10OH^- \rightarrow SeO_3^{2-} + 2SO_4^{2-} + 6I^- + 5H_2O \quad (43)$$

In a bicarbonate medium, sulphurous ion SO_3^{2-} also oxidizes using two mole-equivalents of iodine. The titration by iodine in a bicarbonate medium with preliminary blocking SO_3^{2-} with formalin gives an amount of selenotrithionic acid. Diselenotetrathionic acid by action of bicarbonate decomposes to monoselenotrithionic acid with the release of one mole of Se:

$$Se_2S_2O_6^{2-} \rightarrow Se + SeS_2O_6^{2-} \quad (44)$$

Determining the released Se and monoselenotrithionic acid in the mother solution allows to find the concentration of $H_2SeS_2O_6$ and $H_2Se_2S_2O_6$ in their mixture. Selenous acid was analysed by oxidizing the mixture with I_2 and further titration with sodium thiosulphate:

$$H_2SeO_3 + 4I^- + 4H^+ \rightarrow 2Se + 2I_2 + 3H_2O \quad (45)$$

According to this procedure, the released red elemental selenium was oxidized with elemental Br_2 to H_2SeO_3 and was analysed by the procedure above. The concentration of sulphuric acid was determined turbidimetrically or calculated according to the balance of sulphur in the reaction mixture.

2.2. Glass substrate preparation

The research used Thomas® Environmental Slides glass substrates with one side sandblasted and cut to 10×10×1 mm and 20×20×1 mm. All substrates were washed using liquid soap and distilled water, and dried. Then they were cleaned ultrasonically in an acetone bath by using the Sonoswiss SW 3 H cleaner for 10 min

at 40°C in the sweep mode. All samples were dried in air and then used for layer deposition.

2.3. Copper and indium selenide layer deposition

The copper and indium selenide layers were obtained in three steps plus annealing. Firstly, a selenium layer was formed by submerging a glass substrate into 0.4 mol/l H_2SeO_3 and 1 mol/l $KHSO_3$ 1:1 mixture for 2 h and 3 h at 60°C. Then, the sample was rinsed in distilled water and placed for 10 min in a solution of 0.4 mol/l $CuSO_4$ with the addition of 1% hydroquinone for 10 min and 20 min at 40°C, and 5 min and 10 min at 60°C. It is a mixture of univalent and divalent copper salts which consists of 0.34 mol/l Cu(II) and 0.06 mol/l Cu(I) salt. Later the substrates were rinsed with distilled water and submerged in 0.1 mol/l $InCl_3$ solution for 10 min and 20 min at 40°C; the samples were rinsed in distilled water again and dried over $CaCl_2$. Finally, the samples were annealed for 12 h in an inert nitrogen atmosphere at 100°C.

2.4. Materials

All reagents used in the experiments were chemically and analytically pure commercial reagents. Potassium hydrosulphite ($KHSO_3$) (≥98.0% from Sigma–Aldrich), selenous acid (H_2SeO_3) (99.999% trace metals basis from Sigma–Aldrich), crystalline copper sulphate pentahydrate ($CuSO_4 \cdot 5H_2O$) (crystals and lumps, 99.999% trace metals basis, from Sigma–Aldrich), hydroquinone ($C_6H_4(OH)_2$) (flakes, ≥99% ReagentPlus® from Sigma–Aldrich) and indium(III) chloride ($InCl_3$) (reagent grade, 98%, powder from Sigma–Aldrich) were used for the experiments.

2.5. XRD characterization

X-ray diffraction analysis of the layers deposited on the surface of the glass substrate after each step was performed using a D8 Advance diffractometer (Bruker AXS, Karlsruhe, Germany) operating at the tube voltage of 40 kV and tube current of 40 mA. Diffraction patterns were recorded in a Bragg-Brentano geometry, using a fast counting 1-dimensional detector Bruker LynxEye based on silicon strip technology. The X-ray beam was filtered with a Ni 0.02 mm filter to suppress Cu-k alpha β-radiation and the specimens were scanned over the range of 2θ = 3–70° at a scanning speed of 6° 1/min using a coupled two theta/theta scan type. The diffractometer is supplied together with a software package DIFFRAC.SUITE. X-ray diffractograms of the deposited layers were processed using software packages Search Match, ConvX, Xfit and Microsoft Office Excel.

2.6. XPS characterization

XPS measurements were carried out using the upgraded Vacuum Generator (VG) ESCALAB MKII spectrometer fitted with a new XR4 twin anode to obtain

information about the elemental chemical states and surface composition of the layers deposited on the surface of the glass substrate on. The non-monochromatised MgK_α X-ray source was operated at $h\nu$ = 1253.6 eV with a 300 W power (20 mA/15 kV) and the pressure in the analysis chamber was lower than 5×10^{-7} Pa during spectral acquisition. The spectra were acquired with an electron analyser pass energy of 20eV for narrow scans and the resolution of 0.05 eV and with a pass energy of 100 eV for survey spectra. All spectra were recorded at a 90° take-off angle and calibrated from the hydrocarbon contamination using the C 1s peak at 284.6 eV. The spectra calibration, processing and fitting routines were done using the Avantage software (5.918) provided by Thermo VG Scientific. Core level peaks of Se3d, Cu2p, In3d, O1s, Cl2p and C1s were analysed using a non-linear Shirley-type background and the calculation of the elemental composition was performed on the basis of Scofield's relative sensitivity factors.

2.7. SEM/EDS characterization

The morphological analysis of the Cu-In-Se layer on a glass substrate was executed by applying the Scanning Electron Microscope (SEM) Quanta 200 FEG (FEI, Netherlands). Energy dispersive X-Ray spectroscopy (EDS) was performed using a Bruker XFlash 4030 detector. The standard-less ZAF method was used to quantify elements detected with EDS.

2.8. Band gap characterization

The optical absorption spectra were studied at room temperature using the PerkinElmer Lambda 35 UV/VIS Spectrometer with The Labsphere RSA-PE-20 Diffuse Reflectance Sphere in the range of 400–900 nm. The band gap E_g was calculated using this formula [133]:

$$\alpha h\nu = B\left(h\nu - E_g\right)^n \tag{46}$$

α – absorption coefficient;
$h\nu$ – photon energy;
B – constant associated with absorption;

$$\alpha = \frac{\ln 10 \cdot A}{d} \tag{47}$$

A – absorption;
d – layer thickness;

Layer thickness was not measured and A is proportional to α, so the measured A value was used for calculation. E_g was determined from a modified variation of formula $(\alpha h\nu)^n$ against photon energy $h\nu$. The value of the exponent n denotes the nature of the transition:

n = 2 for direct allowed transitions;
n = 2/3 for direct forbidden transitions;
n = 1/2 for indirect allowed transitions;
n = 1/3 for indirect forbidden transitions.

The linear nature of the plot indicates transition (n = 2). The band gap was calculated by extrapolating the linear part of the plot until it intersects the photon energy axis (A = 0). So, $E_g = hv$, when A = 0.

2.9. AAS characterization

The concentration of selenium, copper and indium in copper and indium selenide layers formed on a glass substrate were determined using the atomic absorption spectrophotometry method. The layers were dissolved in 1:1 concentrated nitric acid and distilled water solution.

Selenium, copper and indium present in the resulting solution were determined by using the atomic absorption spectrometer Shimadzu AA-7000. The used wavelength was λ = 196.0 nm, slit width 1.3 nm, lamp current 23 mA for selenium; wavelength λ = 324.8 nm, slit width 0.7 nm, lamp current 6 mA for copper; and wavelength λ = 303.9 nm, slit width 0.7 nm, lamp current 6 mA for indium. An electrodeless discharge lamp and air-acetylene gas mixture was used for flame. The sensitivity is about 0.5 μg/ml for selenium, 0.09 μg/ml for copper and 0.7 μg/ml for indium for 1 % absorption.

The obtained concentrations were used to calculate the deposited elemental mass for selenium, copper, indium in mg on an area unit of one cm^2. Areas were calculated by weighting each sample and comparing its weight to a weight of 1 m^2 substrate.

3. RESULTS AND DISCUSION

3.1. $H_2Se_nS_2O_6$ synthesis and analysis

Several studies of various cases of above described reactions exist [112, 134]. In study [112], an amount of $CaCO_3$ calculated according the below reaction was added with the aim to precipitate sulphuric acid and the reaction is shown in equation (41). $H_2SeS_2O_6$ was formed at the beginning of the reaction, which further continuously converts to $H_2Se_2S_2O_6$ at room temperature (Fig. 4).

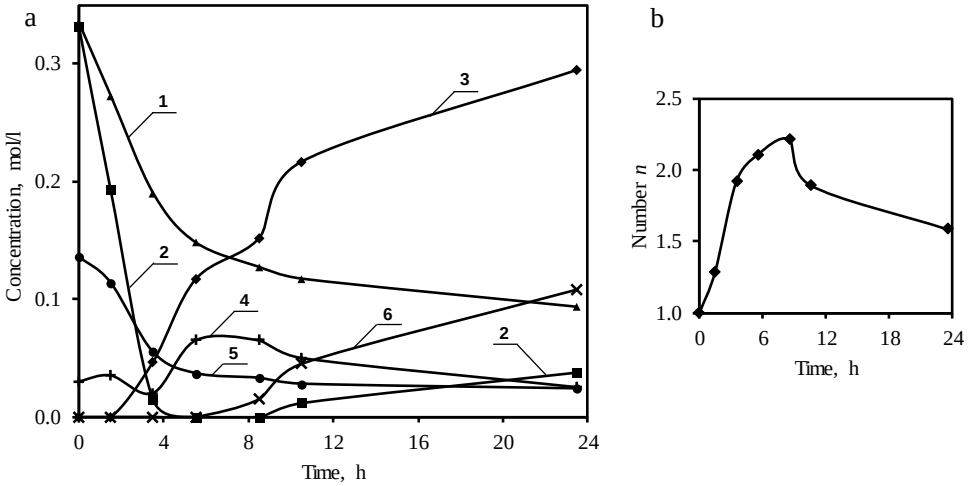

Fig. 4. The kinetics of reaction of H_2SeO_3 and H_2SO_3 at 25°C. 1.4 mol/l H_2SO_3 addition to suspension of $CaCO_3$ in 8 mol/l H_2SeO_3. (a): 1 – $H_2SeS_2O_6$ + $H_2Se_2S_2O_6$, 2 – $H_2SeS_2O_6$, 3 – Se_{el}, 4 – H_2SO_3, 5 – H_2SeO_3, 6 – H_2SO_4. (b): *n* – the number of Se atoms in $H_2Se_nS_2O_6$.

A Small amount of triselenopentathionate acid $H_2Se_3S_2O_6$ also forms, but quickly decomposes. 0.2–0.3 mol/l diselenotetrathionate acid with $H_2Se_3S_2O_6$ (n = 1.9 – 2.1) were found in the reaction solution at 3.5 to 8.5 h from the beginning of the reaction. Decomposition of the formed $H_2Se_2S_2O_6$ to $H_2SeS_2O_6$ with the release of elemental Se begins after 10 h from the beginning of reaction shown in equation (30).

A more detailed study of the reaction of selenous acid with potassium hydrogen sulphite [134] (Fig. 4) was conducted and the reaction is show in equation (42). $H_2SeS_2O_6$ is formed in the first preparation at the beginning of the reaction, with a significant amount (0.03–0.05 mol/l) of $H_2Se_2S_2O_6$. The number of selenium atoms *n* in molecule of $H_2Se_nS_2O_6$ increases continuously from 1.0 to 1.43 with the release of elemental selenium (Fig. 5) during the initial fast stage of reaction.

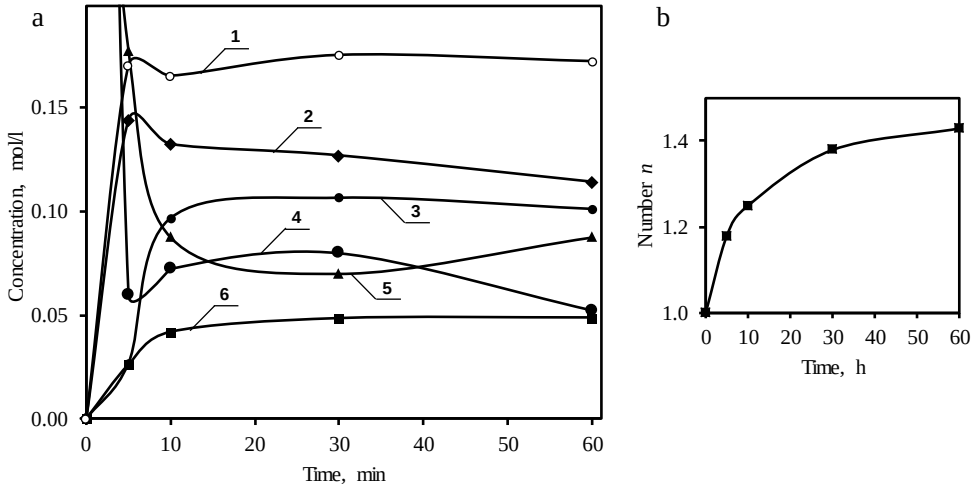

Fig. 5. The kinetics of reaction of H_2SeO_3 and H_2SO_3 at 25°C. 1 mol/l $KHSO_3$ addition to 0.4 mol/l H_2SeO_3. (a): 1 – $H_2SeS_2O_6$ + $H_2Se_2S_2O_6$, 2 – $H_2SeS_2O_6$, 3 – Se_{el}, 4 – H_2SO_3, 5 – H_2SeO_3, 6 – H_2SO_4. (b): *n* – the number of Se atoms in $H_2Se_nS_2O_6$.

Further, the solution changes colour to orange, then to red with the formation of colloidal amorphous selenium. The solution can be stable for weeks, if refrigerated.

$H_2SeS_2O_6$ is formed in the second preparation at the beginning of the reaction, together with a small amount (0.00125–0.031 mol/l) of $H_2Se_2S_2O_6$. The average number of atoms of selenium *n* in a molecule of $H_2Se_nS_2O_6$ during the initial fast stage (one hour from the mixing of reagents) of reaction remains ~ 1.0 (1.00–1.17). The second preparation allow us to prepare almost 99.3% of $H_2SeS_2O_6$ (Fig. 6) only with insignificant release of elemental selenium.

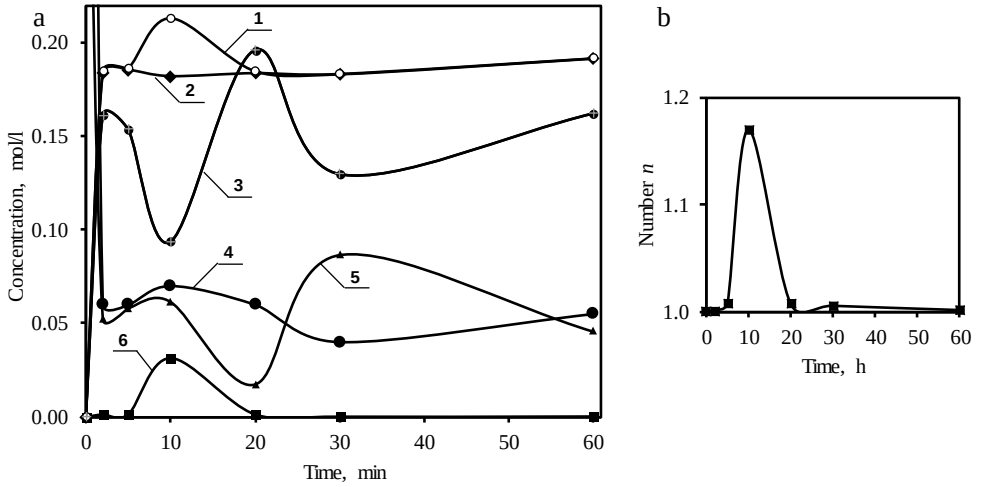

Fig. 6. The kinetics of reaction of H_2SeO_3 and H_2SO_3 at 0°C. 0.4 mol/l H_2SeO_3 addition to 1 mol/l $KHSO_3$. (a): 1 – $H_2SeS_2O_6$ + $H_2Se_2S_2O_6$, 2 – $H_2SeS_2O_6$, 3 – Se_{el}, 4 – H_2SO_3, 5 – H_2SeO_3, 6 – $H_2Se_2S_2O_6$. (b): n – the number of Se atoms in $H_2Se_nS_2O_6$.

Further, the reaction kinetics was investigated at 25°C using thermostatic arrangement. Monoselenotrithionate acid $H_2SeS_2O_6$ starts to decompose to $H_2Se_2S_2O_6$ (n = 1.04 – 1.40) with a release of elemental selenium only after 20 h (Fig. 7).

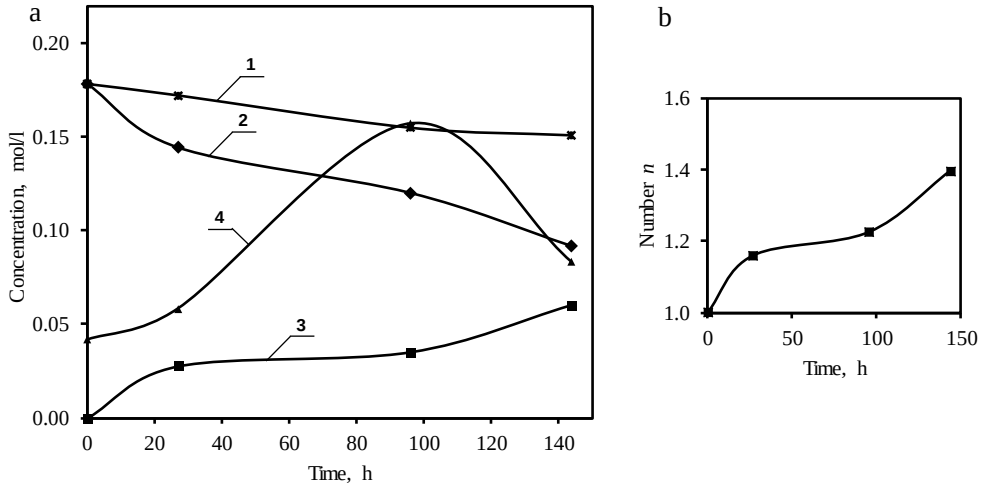

Fig. 7. The kinetics of reaction of H_2SeO_3 and H_2SO_3 at 25°C. 0.4 mol/l H_2SeO_3 addition to 1 mol/l $KHSO_3$. (a): 1 – $H_2SeS_2O_6$ + $H_2Se_2S_2O_6$, 2 – $H_2SeS_2O_6$, 3 – $H_2Se_2S_2O_6$, 4 – H_2SO_3. (b): *n* – the number of Se atoms in $H_2Se_nS_2O_6$.

Several studies of various cases describing the reaction and interpretation of its mechanism exist [105, 135, 136]. However, the reaction suffers from a serious limitation, because of the inability to exactly determine its mechanism because of its

complexity. The reaction may have two stages. Firstly, during the fast initial stage $H_2SeS_2O_6$ and $H_2Se_2S_2O_6$ acids form (reactions (17) and (18)). The second stage is slower decomposition of both $H_2SeS_2O_6$ and $H_2Se_2S_2O_6$ through a number of reactions ((23)–(29)) with the formation of elemental selenium, H_2SO_3 and H_2SO_4. The formed H_2SO_3 then may react with the excess H_2SeO_3 to form more elemental selenium (equation (16)). Furthermore, selenium and H_2SO_3 can react and regenerate $H_2Se_2S_2O_6$ (equation (19)), which then again decomposes back to elemental selenium, H_2SO_3 and H_2SO_4. These processes may explain various concentration fluctuations during the reaction.

The reaction rate depends on temperature and the concentration of the initial solution. According to the kinetics curves, some characteristics of three types of reaction were calculated (Table 3).

Table 3. Kinetic characteristics for $H_2Se_nS_2O_6$ (n = 1–2) formation at 0 and 25°C

Reaction type	Ratio of concentrations, mol/l H_2SeO_3:H_2SO_3	Tempe-rature, °C	Rate law	Average rate constant k 10^3, s^{-1}
Addition of H_2SO_3 to the suspension of $CaSeO_3$	0.08:0.2	0	$v = k_t [H_2SeO_3]$	4.6 10^{-2}
Addition of $KHSO_3$, to an excess of H_2SeO_3	0.02:0.05	25	$v = k_t [H_2SeO_3]$	1.85
Addition of H_2SeO_3 to an excess of $KHSO_3$	0.02:0.05	0	$v = k_t [H_2SeO_3]$	5.09

As the reaction is very complicated, the isolation method was applied in conjunction with the method of initial rates [137]. The method of initial rates might not reveal the entire rate law because in a complex reaction the products themselves might affect the rate. That is in the case of the formation of monoselenotrithionate $H_2SeS_2O_6$ and diselenotetrathionate $H_2Se_2S_2O_6$ acids the decomposition of which through unstable intermediate product H_2SeSO_3 or known [135] sulphurous decomposition of diselenotetrathionate acid leads to the regeneration of initial reagents, such as H_2SO_3:

$$H_2Se_nS_2O_6 + H_2O \rightarrow nSe + H_2SO_4 + H_2SO_3 \quad (48)$$

The kinetics of three types of $H_2Se_nS_2O_6$ formation process were studied and analysed. The first-order rate expression was tested by plotting $\ln c_{H_2SeO_3}$ against time, a plot of $1/c_{H_2SeO_3}$ against time, based on the assumption of a second-order mechanism, and a plot of $1/c^2_{H_2SeO_3}$. All three mechanisms were tested for all three types of reaction. Calculations show that the correlation coefficient values, R^2 for the first-order rate law (0.9724–0.9984) are greater than the correlation coefficients of other two plots, (respectively, 0.9133–0.9603 and 0.8238–0.9164) for all three types of studied

reactions. The data of the reaction with the addition of $KHSO_3$ to an excess of H_2SeO_3 show the best agreement with the first-order mechanism. The regression coefficients for the linear plots were highest ($R^2 = 0.9984$) among all type of reactions in this study. It suggests that the preferred mechanism of the first stage of reaction is first-order rather than second-order. Also, the data for the first-order rate law were only analysed for the 10–20 minutes of $H_2Se_nS_2O_6$ formation reactions. After this initial reaction part, the deviation from the linear curve increased rapidly. Kinetic calculations allow us to assume that the reaction with the rate law of the form $v = k_t[H_2SeO_3]$ corresponds to the first-order reaction. The integrated rate law of a reaction may be expressed as:

$$[H_2Se_nS_2O_6] = [H_2SeO_3]_0(1 - e^{-kt}) \quad (49)$$

$[H_2Se_nS_2O_6]$ – the concentration of formed selenopolythionic acid at time t; $[H_2SeO_3]_0$ – the initial concentration of selenous acid; k_t – rate constant.

The mechanism and kinetic characteristics of this reaction were compared with the already investigated and known properties of stability of monoselenotrithionate $H_2SeS_2O_6$ and diselenotetrathionate $H_2Se_2S_2O_6$ isolated from their potassium salts [112, 138] (Fig. 8, Fig. 9).

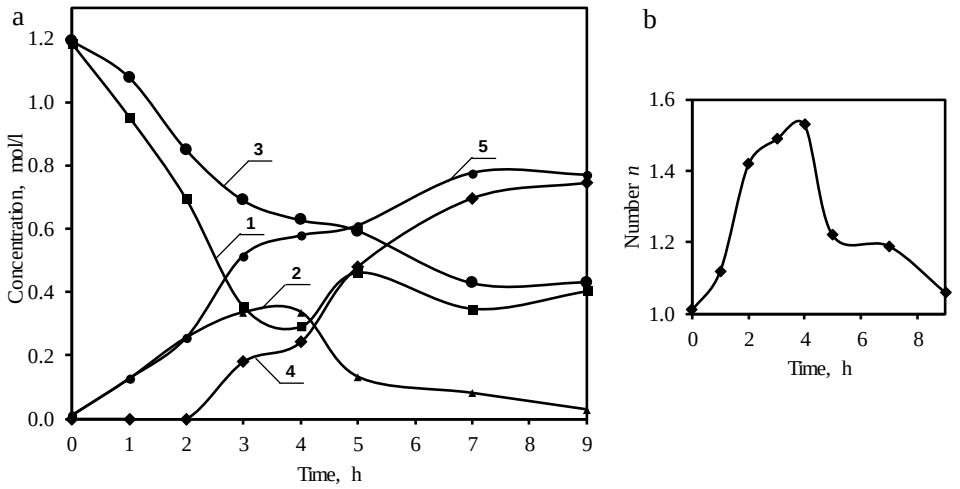

Fig. 8. The kinetics of decomposition of $H_2SeS_2O_6$ 1.02 mol/l at 25°C. (a): 1 – $H_2SeS_2O_6$, 2 – $H_2Se_2S_2O_6$, 3 – $H_2SeS_2O_6$ + $H_2Se_2S_2O_6$, 4 – Se_{el}, 5 – H_2SO_4. (b): *n* – the number of Se atoms in $H_2Se_nS_2O_6$

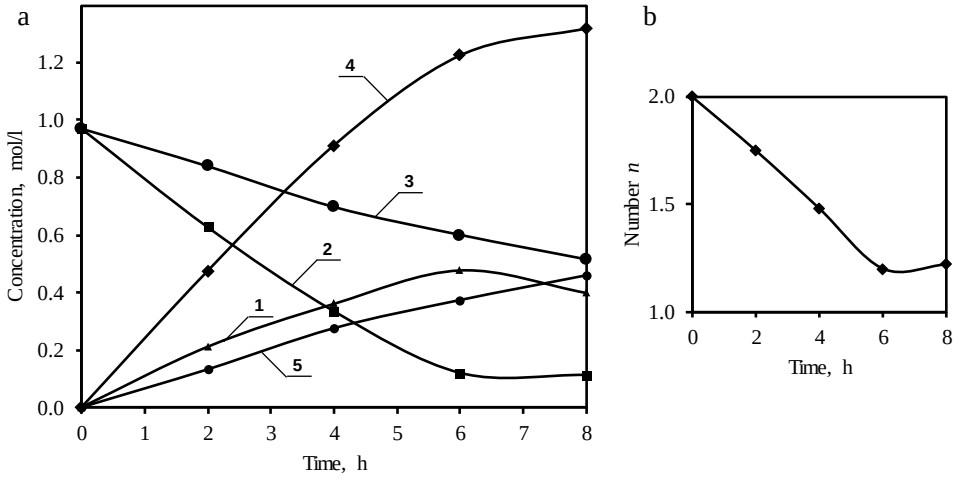

Fig. 9. The kinetics of decomposition of $H_2Se_2S_2O_6$ 0.97 mol/l at 25°C. (a): 1 – $H_2SeS_2O_6$, 2 – $H_2Se_2S_2O_6$, 3 – $H_2SeS_2O_6$ + $H_2Se_2S_2O_6$, 4 – Se_{el}, 5 – H_2SO_4. (b): *n* – the number of Se atoms in $H_2Se_nS_2O_6$

Table 4 summarizes the known kinetic characteristics of selenopolythionate acids and its potassium salts. The stability of selenopolythionate acid decreases with the increasing number of selenium atoms in an acid molecule. Table 4 shows the values of the first-order rate constant, *k*, were found to increase four-fold for $H_2Se_2S_2O_6$ in comparison to $H_2SeS_2O_6$ from 2.98 10^{-6} s^{-1} to 10.6 10^{-6} s^{-1}, approximately for the same initial concentration, respectively, 0.190 mol/l and 0.247 mol/l.

Table 4. Rates of decomposition for $H_2Se_nS_2O_6$ (n = 1–2) at 25°C, $K_2SeS_2O_6$ at 20°C and 30°C

Selenopolythionate compound	Concentration, mol/l	Half – life, $\tau_{½}$, h	Average rate constant k 10^6, s^{-1}
$H_2SeS_2O_6$	1.02	2.6	63.5
	0.375		6.38
	0.190	42	2.98
$H_2Se_2S_2O_6$	0.972	3	76.6
	0.603		25.7
	0.247	16	10.6
$K_2SeS_2O_6$* [138]	0.0488	112	1.64
$K_2SeS_2O_6$** [138]	0.0452	22	7.88
$K_2SeS_2O_6$*** [138]	0.0396	75	2.70

* in distilled water at 30°C;

** in 0.1 mol/l HCl at 30°C;

*** in 0.1 mol/l HCl at 20°C

The comparison of data for potassium selenotrithionate decomposition (Table 4) shows that the decomposition rate and isolation of elemental Se depends on the acidity of the solution. In acidified solutions (pH = 1.1), the isolation of Se starts after 45 h from the beginning of decomposition at 30°C, in distilled water (pH = 7.0), respectively, after 120 h. First-order decomposition rate constants calculated for the first stage of decomposition show that $K_2SeS_2O_6$ decomposes approximately five times faster in an acidic solution than in distilled water at 30°C. The data also [136] show an increase of decomposition rate of $K_2SeS_2O_6$ in acidified solutions with temperature. Table 4 indicates that the values of the first-order rate constant, k, were found to increase from 2.70 10^{-6} s^{-1} to 7.88 10^{-6} s^{-1}, with an increase of the solution temperature from 20°C to 30°C. Again, the average value of temperature coefficients of $K_2SeS_2O_6$ decomposition is 2.90 to 3.06, which corresponds to first-order reactions [136].

Quantitative data on the decomposition kinetics of potassium diselenotetrathionate are not available. $K_2Se_2S_2O_6$ is more stable in slightly acidified solutions, but completely decomposes to elemental selenium and sulfuric acid in acidic solutions, as shown in equation (28).

Some difficulties occur in comparing the kinetic data for decomposition of selenopolythionate acids and its potassium salts due to the differences in concentrations and temperature. However, it might be stated that the stability of selenopolythionate acids is significantly higher than the stability of its potassium salts even at higher concentrations (Table 4). This feature shows that selenopolythionate acids are more convenient in longer selenization processes even though both, acids and salts, possess almost the same purity and decomposition products. Nevertheless,

the elemental composition of acids (32.75–49.36% of Se in acids against 24.73–39.66% of Se in its potassium salts) helps to increase the amount of Se in selenized surface layer of the substrate.

Direct reactions of isolation of selenopolythionate compounds showed a strong dependence upon the conditions of reactions: temperature, admixtures and duration. An addition of $CaCO_3$ allows increasing the concentration of diselenotetrathionate acid ten-fold. The use of $KHSO_3$ instead of H_2SO_3 allows increasing the concentration of the resulting solution of selenotrithionate and of diselenotetrathionate acids to ~ 0.2 mol/l and its stability as H_2SO_4 was eliminated.

The amount of elemental Se is, respectively, 33.64, 40.54 and 49.65% in synthesized precursors $H_2Se_nS_2O_6$ (n = 1.04, 1.40 and 2.1) using three types of direct reactions, which shows similar enrichment with Se compared to selenotrithionate and diselenotetrathionate acids (a 10% increase compared to potassium salts).

An estimation of direct experimental reaction rates and the calculation of reactions rate constants showed us that the most suitable process for selenization, especially for the CBD procedure on glass substrates, is fast reaction of selenous acid and $KHSO_3$. The superiority of easy selenopolythionate anion $Se_nS_2O_6^{2-}$ production in direct experiments compared to its preparation in the form of potassium salts, or even longer isolation from potassium salts in the form of selenopolythionate acids, makes this type of selenopolythionate precursor preparation especially attractive for selenization.

3.2. Selenium layer on glass

3.2.1. XRD analysis

Fig. 10 shows the XRD patterns of elemental selenium layers on the glass substrate obtained during the first step of their formation process. The glass substrate was submerged into a mixture of solutions H_2SeO_3 and $KHSO_3$ at 60°C for two (pattern (a)) and three (pattern (b)) hours. Only one peak (+) at 2θ = 23.5° phase of monoclinic selenium (JCPDS: 24-714) appears (Table 6). The three-hour deposition pattern (b) shows a slightly more intense peak than the two-hour deposition pattern (a), indicating that more elemental selenium was deposited on the glass substrate. Only a single selenium peak indicates that the majority of selenium is in the amorphous phase, which is red in colour. It is known that red amorphous selenium is more active than black crystalline selenium [139]. This is why amorphous selenium should react more actively with copper ions. This pattern confirms that elemental selenium is formed and these reactions take place in the precursor solution, as shown in equations (42) and (44).

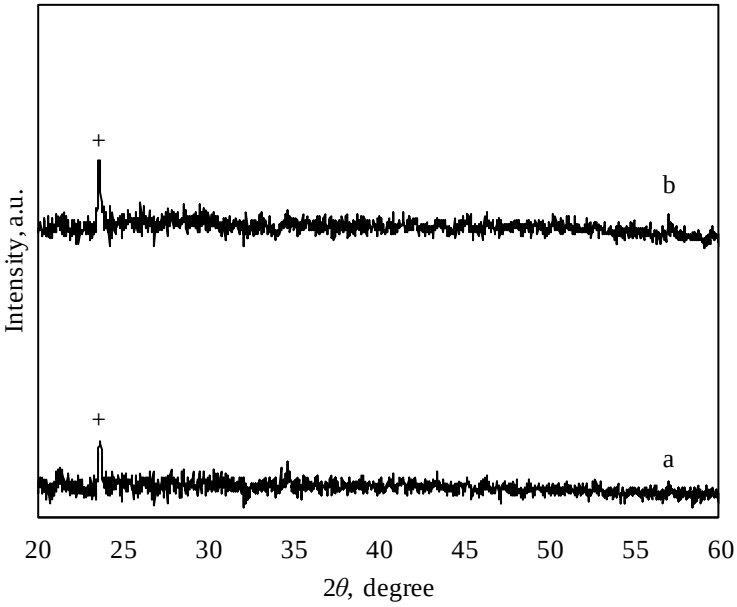

Fig. 10. XRD patterns of selenium layers on a glass substrate for 2 (a) and 3 (b) hours. The peak was identified as (+) – Se (24-714) monoclinic selenium.

3.2.2. XPS analysis

To get more information about the formation of the selenium layer on the glass substrate, it was analysed by using X-ray photoelectron spectroscopy (XPS). The surface layer was obtained during the first step, when the glass substrate was submerged into a mixture of solutions H_2SeO_3 and $KHSO_3$. The surface layer and its deeper areas were studied as well after etching.

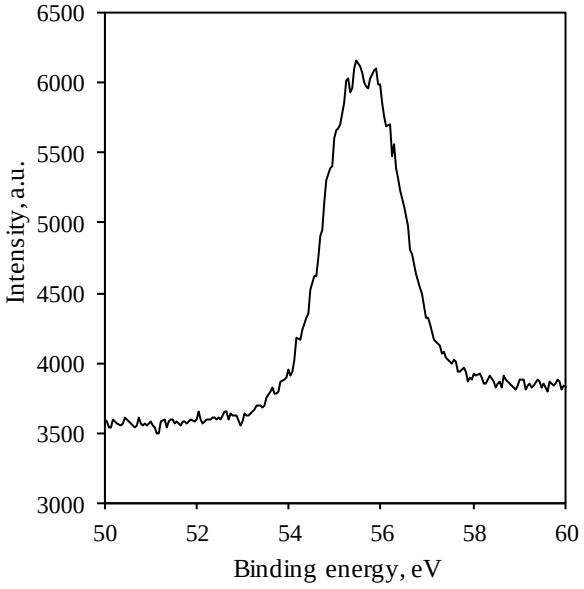

Fig. 11. High resolution XPS spectra in $Se3d_{5/2}$ region of the etched elemental selenium layer on a glass substrate. Sample selenized for 3 hours.

The signal of the etched selenium layer on glass can be seen in Fig. 11. It exhibits a signal at 55.7 eV (Table 7) which corresponds to selenium in elemental state (Se^0) [140].

3.3. Copper selenide layer on glass

3.3.1. XRD analysis

During the second stage, the glass substrate with a layer of elemental selenium was submerged into $CuSO_4$ and hydroquinone solution. Peaks corresponding to the phase of monoclinic selenium shown in Fig. 10 (pattern (a) and (b)) disappear. This indicates that selenium has reacted with Cu(I) ions and formed a copper selenide layer.

Samples which were selenized for two hours show four new peaks (◊) at 2θ = 26.6, 28.1, 31.1 and 50.0° of copper selenide phase – hexagonal klockmannite $Cu_{0.87}Se$ (JCPDS: 83-1814) (Table 6) in Fig. 12 (a) (pattern (1), (2) and (3)). However, considering another copper selenide phase – cubic berzelianite $Cu_{2-x}Se$ (JCPDS: 6-680) (Table 6) peaks appear at 2θ = 26.75, 44.6, 52.9° (pattern (4)).

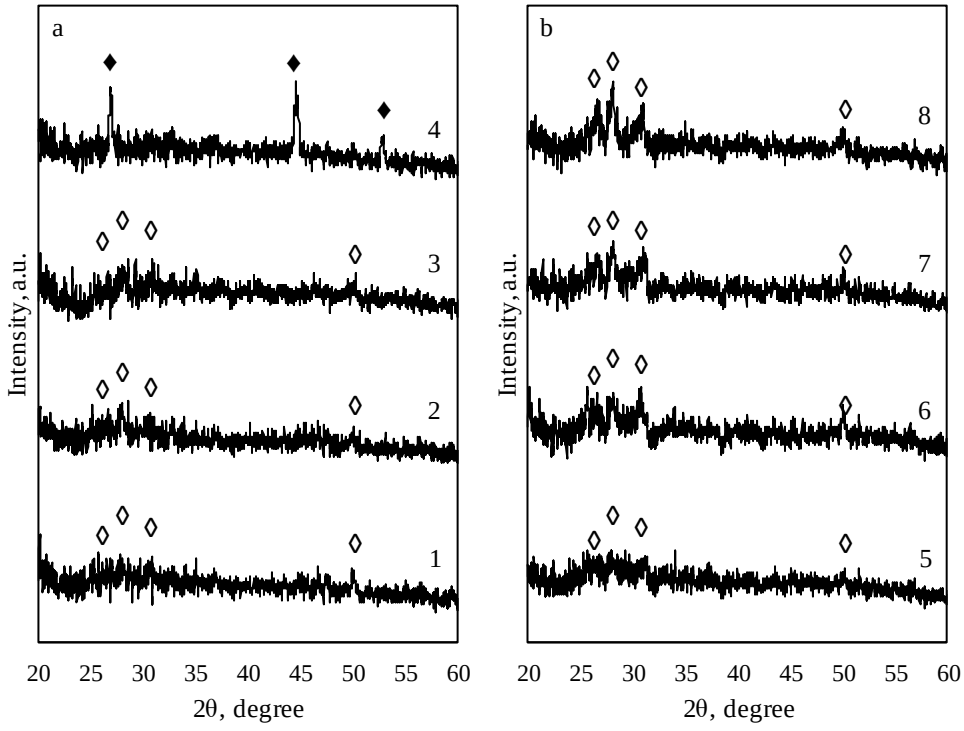

Fig. 12. XRD patterns of copper selenide layers on a glass substrate. The peaks were identified as (◊) – $Cu_{0.87}Se$ (83-1814) hexagonal klockmannite and (♦) – $Cu_{2-x}Se$ (6-680) cubic berzelianite. Samples were selenized: (a) – 2 hours and (b) – 3 hours. The temperature and duration of copper(I/II) salt solution treatment: 1, 5 – 10 min at 40°C; 2, 6 – 20 min at 40°C; 3, 7 – 5 min at 60°C; 4, 8 – 10 min at 60°C.

Similar results for samples that were selenized for three hours can be seen in Fig. 12 (b): the monoclinic selenium peak also disappears and hexagonal klockmannite $Cu_{0.87}Se$ peaks appear as mentioned above, but in all four patterns ((1), (2), (3) and (4)). Also, no cubic berzelianite $Cu_{2-x}Se$ peaks have been found to form when selenization lasts 3 hours (Fig. 12 (b)). All graphs indicate (Fig. 12) that higher treatment temperature (60°C vs. 40°C) and longer durations (20 min vs. 10 min and 10 min vs. 5 min) seem to yield layers with more intense peaks, thus indicating more copper selenide formed.

The disappearance phase of monoclinic selenium and the appearance of new copper selenide phases indicate that the reaction of the formation of copper selenides Cu_xSe ($Cu_{2-x}Se$ and $Cu_{0.87}Se$) has taken place which is described in equation:

$$Se + 2xCu^{+} \rightarrow Cu_xSe + xCu^{2+} \tag{50}$$

3.3.2. AAS analysis

Atomic absorption spectroscopy analysis method was used to determine amount of selenium and copper and shown in Table 5.

Samples submerged into mixture of solutions H_2SeO_3 and $KHSO_3$ at 60 °C for 2 hours have less selenium (1.201–1.230 μmol/cm^2) compared to the 3 hour selenization samples (2.861–2.924 μmol/cm^2). Data here coincide with XRD data (Fig. 10), 3 hours selenized sample has more intense elemental selenium peak.

Copper(I/II) salt solution treatment with temperature and durations seems to have impact on the amount of copper in the layers. The longer the copper(I/II) salt solution treatment duration and the higher treatment temperature, the more copper react with deposited selenium layers. Samples that were treated for 10 min (0.787 and 0.861 μmol/cm^2) have less copper than the 20 min ones at 40 °C (0.868 and 0.933 μmol/cm^2). Also, 5 min samples (0.903 and 0.950 μmol/cm^2) have less copper compared to 10 min samples (0.922 and 1.028 μmol/cm^2) at 60 °C. Furthermore, 40 °C samples (0.787 and 0.861 μmol/cm^2) have less copper than 60 °C samples (0.922 and 1.028 μmol/cm^2) with the same 10 min treatment duration. The discussed results line up with XRD data (Fig. 12) as well, higher temperature and longer copper(I/II) salt solution treatment durations seems to produce more intense copper selenide (hexagonal klockmannite $Cu_{0.87}Se$ and cubic berzelianite $Cu_{2-x}Se$) peaks.

Table 5. Calculated amounts of selenium and copper in copper selenide layers

Conditions of treatments					Amount of elements, μmol/cm^2	
					Se	Cu
Selenization	2 h	copper(I/II) salt solution treatment	40 °C	10 min	1.209	0.787
				20 min	1.201	0.868
			60 °C	5 min	1.230	0.903
				10 min	1.227	0.922
	3 h		40 °C	10 min	2.924	0.861
				20 min	2.899	0.933
			60 °C	5 min	2.886	0.950
				10 min	2.861	1.028

3.4. Copper and indium selenide layer on glass

3.4.1. XRD analysis

All obtained copper selenide layers were submerged into an indium(III) salt solution for 10 min (Fig. 13) and 20 min (Fig. 14) at 40°C. In neither of the samples (except Fig. 13, pattern 4) new peaks disappeared; however, one new cubic indium selenide In_2Se_3 (JCPDS: 20-492) peak (●) at 2θ = 46.0° appeared on all samples (Fig. 13 and Fig. 14, except Fig. 13 pattern 4). This indicates the formation of a new phase of indium selenide according equations:

$$3CuSe + 2In^{3+} \rightarrow In_2Se_3 + 3Cu^{2+} \quad (51)$$

$$3Cu_2Se + 2In^{3+} \rightarrow In_2Se_3 + 6Cu^{+} \quad (52)$$

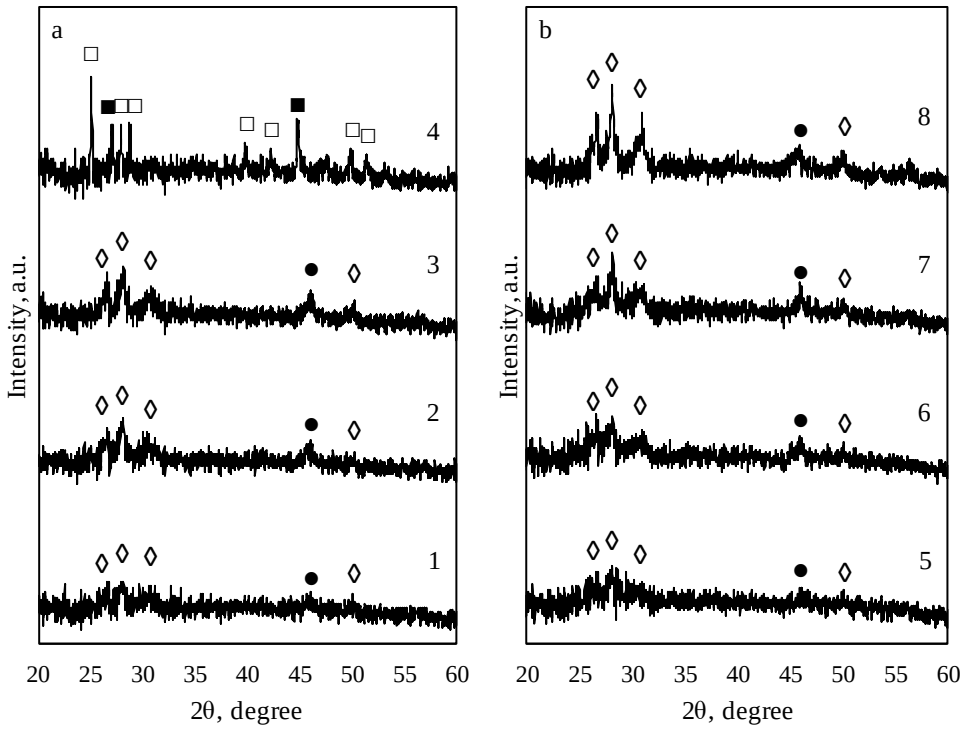

Fig. 13. XRD patterns of copper and indium selenide layers on a glass substrate. The peaks were identified as (◊) – $Cu_{0.87}Se$ (83-1814) hexagonal klockmannite; (□) – Cu_3Se_2 (71-45) tetragonal umangite; (■) – Cu_7Se_4 (26-557) cubic copper selenide; (●) – In_2Se_3 (20-492) cubic indium selenide. Samples selenized: (a) – 2 hours and (b) – 3 hours. The temperature and duration of Copper(I/II) salt solution treatment: 1, 5 – 10 min at 40°C; 2, 6 – 20 min at 40°C; 3, 7 – 5 min at 60°C; 4, 8 – 10 min at 60°C. 10 min indium(III) salt solution treatment.

In this sample (Fig. 13, pattern 4), all three $Cu_{2-x}Se$ cubic berzelianite peaks disappeared (this was present before in Fig. 12, pattern 4) and two new phases were

formed. The first one is tetragonal umangite Cu_3Se_2 (JCPDS: 71-45) (Table 6) which has seven peaks (□) at 2θ = 25.0, 27.8, 28.7, 39.8, 42.2, 49.8, 51.3°. The other phase is cubic copper selenide Cu_7Se_4 (JCPDS: 26-557) (Table 6) which has two peaks (■) at 2θ = 27.1, 44.9° (Fig. 13, pattern 4). This sample has no indium containing phases or the phase is amorphous.

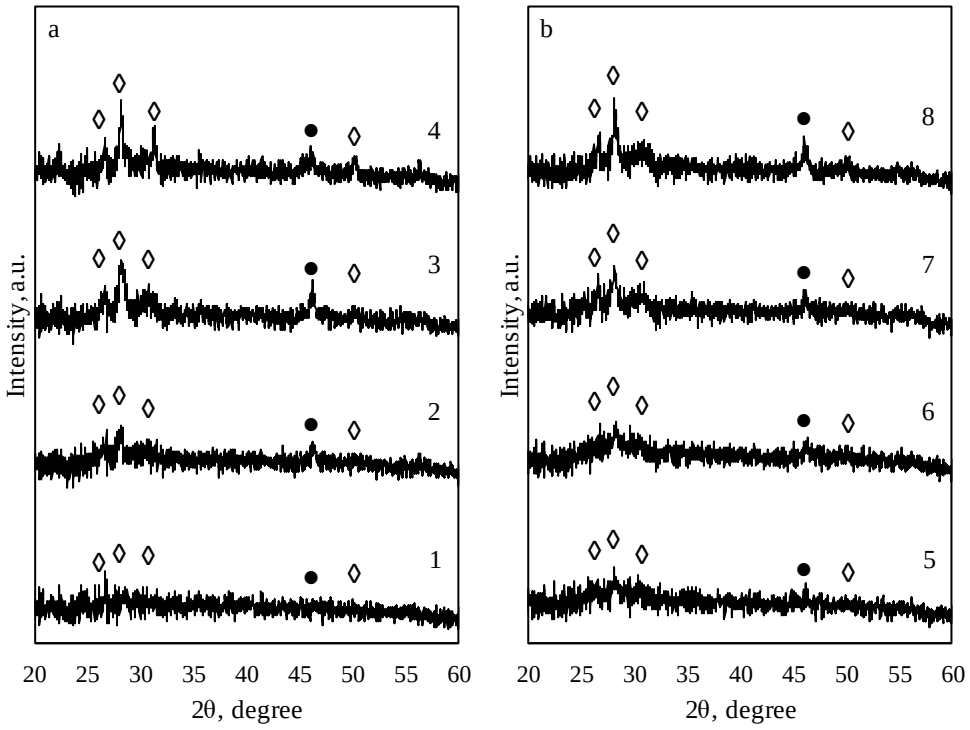

Fig. 14. XRD patterns of copper and indium selenide layers on a glass substrate. The peaks were identified as (◊) – $Cu_{0.87}Se$ (83-1814) hexagonal klockmannite; (●) – In_2Se_3 (20-492) cubic indium selenide. Samples were selenized: (a) – 2 hours and (b) – 3 hours. The temperature and duration of copper(I/II) salt solution treatment: 1, 5 – 10 min at 40°C; 2, 6 – 20 min at 40°C; 3, 7 – 5 min at 60°C; 4, 8 – 10 min at 60°C. 20 min indium(III) salt solution treatment

All other samples (Fig. 13 patterns 1–3, 5–8 and Fig. 14) show intensive and clear characteristic peaks of the $Cu_{0.87}Se$ which indicate that the layer formed after the third step consists mostly of $Cu_{0.87}Se$ phase and small amounts of In_2Se_3 phase. Higher peaks show that these phases tend to form better when the copper(I/II) salt solution treatment is done at 60°C (Fig. 13 patterns 3, 7, 8 and Fig. 14, patterns 3, 4, 7, 8) than at 40°C. The results of this research show that annealing is needed to obtain the $CuInSe_2$ phase.

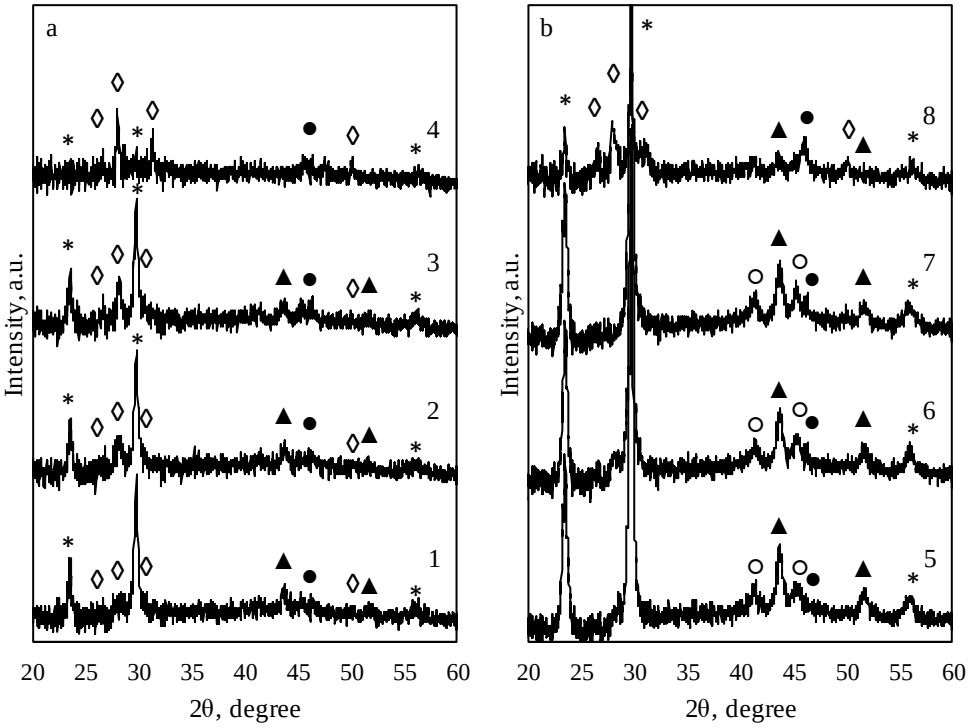

Fig. 15. XRD patterns of copper and indium selenide layers on a glass substrate. The peaks were identified as (*) – Se (73-465) hexagonal selenium; (◊) – $Cu_{0.87}Se$ (83-1814) hexagonal klockmannite; (●) – In_2Se_3 (20-492) cubic indium selenide; (○) – In_2Se_3 (17-356) indium selenide; (▲) – $CuInSe_2$ (23-207) cubic copper indium selenide. Samples were selenized: (a) – 2 hours and (b) – 3 hours. The temperature and duration of copper(I/II) salt solution treatment: 1, 5 – 10 min at 40°C; 2, 6 – 20 min at 40°C; 3, 7 – 5 min at 60°C; 4, 8 – 10 min at 60°C. 10 min indium(III) salt solution treatment and annealing

Finally, all samples were annealed for 12 h in an inert (nitrogen) atmosphere at 100°C. The process promotes the appearance of a lot of new phases. Three new peaks (*) at 2θ = 23.5, 29.7 and 56.3° of hexagonal selenium (JCPDS: 73-465) (Table 6) are found across all samples. This indicates that amorphous elemental selenium has changed to crystal phase. Naturally, samples that have been submerged into a mixture of solutions H_2SeO_3 and $KHSO_3$ for two hours (Fig. 15 (a) and Fig. 16 (a)) have lower peaks compared to the ones that were selenized for three hours. (Fig. 15 (b) and Fig. 16 (b)). Also, hexagonal selenium patters are almost non-existent in samples that were treated with copper (II/I) salt solution for 10 min at 60°C (Fig. 15 pattern 4 and Fig. 16 pattern 4) same two-hour selenization, which shows that almost all selenium reacted with other phases. The same two samples (Fig. 15 pattern (8) and Fig. 16 pattern (8)) have much lower peaks than the remaining samples (Fig. 15 pattern (5),

(6), (7) and Fig. 16 pattern (5) , (6), (7)) indicating that much of the selenium reacted with other phases as well.

It appears that in most samples (except Fig. 15 pattern (4)), hexagonal klockmannite $Cu_{0.87}Se$ peaks (◊) are lower (Fig. 15 pattern (1), (2), (3), (8); Fig. 16 pattern (3), (4), (7), (8)) or disappear completely (Fig. 15 pattern (5), (6), (7); Fig. 16 pattern (1), (2), (5), (6)). This shows that copper selenide phase – hexagonal klockmannite $Cu_{0.87}Se$ reacted with other phases.

Similarly to klockmannite after annealing, indium selenide (JCPDS: 20-492) in most cases (except Fig. 15 pattern (4)) shows lower peaks (Fig. 15 pattern (1), (2), (3), (5), (6), (7) (8); Fig. 16 pattern (3), (4), (7), (8)) or peaks disappear completely (Fig. 16 pattern (1), (2), (5), (6)). This also indicates that the indium selenide phase reacted with other phases.

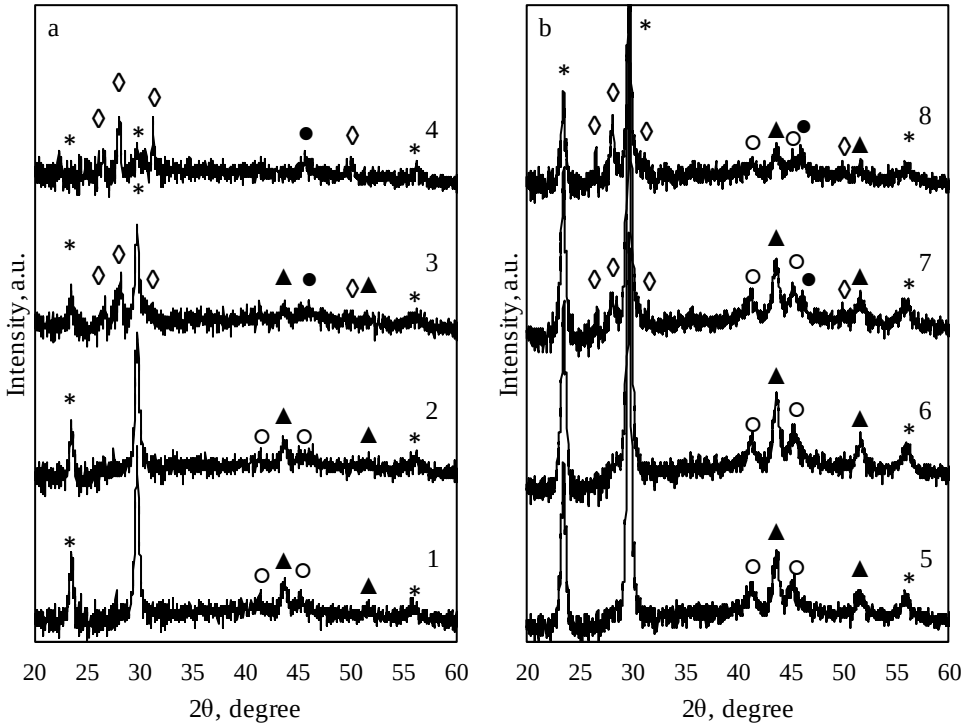

Fig. 16. XRD patterns of copper and indium selenide layers on a glass substrate. The peaks were identified as (*) – Se (73-465) hexagonal selenium; (◊) – $Cu_{0.87}Se$ (83-1814) hexagonal klockmannite; (●) – In_2Se_3 (20-492) cubic indium selenide; (○) – In_2Se_3 (17-356) indium selenide; (▲) – $CuInSe_2$ (23-207) cubic copper indium selenide. Samples were selenized: (a) – 2 hours and (b) – 3 hours. The temperature and duration of copper(I/II) salt solution treatment: 1, 5 – 10 min at 40°C; 2, 6 – 20 min at 40°C; 3, 7 – 5 min at 60°C; 4, 8 – 10 min at 60°C. 20 min indium(III) salt solution treatment and annealing

Meanwhile, after annealing, two diffraction peaks (▲) at 2θ = 43.6, 51.8° of cubic copper indium selenide phase $CuInSe_2$ (JCPDS: 23-207) (Table 6) and two diffraction peaks (○) at 2θ = 41.3, 45.3° of the new phase of indium selenide In_2Se_3 (JCPDS: 17-356) (Table 6) appear. Very similarly to elemental selenium phase, samples that have been selenized for two hours (Fig. 15 (a) and Fig. 16 (a)) have lower or no peaks compared to the ones that were selenized for three hours (Fig. 15 (b) and Fig. 16 (b)). Both phases show lower or no peaks when selenization lasted two hours: no copper indium selenide can be found on two-hour selenization samples that were treated with copper(I/II) salt solution for 10 min at 60°C (Fig. 15 pattern (4) and Fig. 16 pattern (4)) and minimal amounts are found on the same three-hour selenization samples (Fig. 15 pattern (8) and Fig. 16 pattern (8)).

Similarly, no indium selenide (JCPDS: 17-356) peaks are found in Fig. 15 pattern (1), (2), (3), (4), (5) and Fig. 16 pattern (3), (4), minimal peaks are in Fig. 16 pattern (1), (2), (8).

The highest peaks of both copper indium selenide and indium selenide are found when the samples were selenized in a selenium precursor for three hours and copper(I/II) salt treatment was both 10 min and 20 min at 40°C and 5 min at 60°C (Fig. 15 pattern (5), (6), (7) and Fig. 16 pattern (5), (6), (7)).

These results can be illustrated by solid-state reactions which are described by the following equations:

$$2CuSe + In_2Se_3 \rightarrow 2CuInSe_2 + Se \quad (53)$$

$$Cu_2Se + In_2Se_3 \rightarrow 2CuInSe_2 \quad (54)$$

This is how phases of hexagonal selenium (JCPDS: 73-465) and copper indium selenide (JCPDS: 23-207) are formed. Also, as a result of these reactions, the amount of phase of copper selenide $Cu_{0.87}Se$ (JCPDS: 83-1814) decreases significantly.

It is possible that selenium and the cation of univalent copper had formed during equations (52), (53), and this reaction:

$$2Cu_2Se + In^{3+} \rightarrow CuInSe_2 + 3Cu^{+} \quad (56)$$

They react according to equation (50), and copper selenide is formed. Then copper selenide reacts with In^{3+} cations, as shown in equations (51) and (52).

An exchange of ions is possible because the solubility product for In_2Se_3 is $5.6 \cdot 10^{-92}$ $mol^5 \cdot dm^{-15}$, while the solubility products for CuSe and Cu_2Se are $1.4 \cdot 10^{-36}$ $mol^2 \cdot dm^{-6}$ and $1.1 \cdot 10^{-51}$ $mol^3 \cdot dm^{-9}$, respectively [141]. Thus, indium selenide (JCPDS: 17-356) phase is formed.

It appears that the optimal conditions for obtaining copper indium selenide phase are: three-hour selenization followed by copper(I/II) salt treatment, both 10 min and 20 min at 40°C and 5 min at 60°C, followed by indium chloride 10 min and 20 min treatment at 40°C and finally annealing at 100°C in an inert nitrogen atmosphere.

A two-hour selenization may not be optimal due to the lack of elemental selenium deposited. Also, copper selenide treated at 60°C tends to form unwanted $Cu_{0.87}Se$ hexagonal klockmannite phase. While a 5 min treatment results in high copper indium selenide and indium selenide peaks, small amounts of klockmannite peaks can be found as well.

To improve the small amounts of desired copper indium selenide phase, further optimisations and corrections of layer formation process is needed.

Table 6. XRD 2Θ peaks and their assignment to the formed layers on a glass substrate using the SILAR method

	Name	Formula	System	JCPDS	2-Theta	Literature
+	Se	selenium	monoclinic	24-714	23.523	[142]
◊	$Cu_{0.87}Se$	klockmannite	hexagonal	83-1814	26.615, 28.107, 31.082, 50,000	[143]
♦	$Cu_{2-x}Se$	berzelianite	cubic	6-680	26.750, 44.600, 52.913	[144]
□	Cu_3Se_2	umangite	tetragonal	71-45	25.011, 27.847, 28.685, 39.790, 42.209, 49.784, 51.325	[145]
■	Cu_7Se_4	copper selenide	cubic	26-557	27.081, 44.903	[146]
●	In_2Se_3	indium selenide	cubic	20-492	46.048	[147]
*	Se	selenium	hexagonal	73-465	23.520, 29.700, 56.252,	[148]
▲	$CuInSe_2$	copper indium selenide	cubic	23-207	43.752	[5]
○	In_2Se_3	indium selenide	unknown	17-356	28.569, 41.321, 45.302	[147]

3.4.2. XPS analysis

The high-resolution XPS spectra of Se3d, Cu2p and In3d regions of unetched copper and indium selenide layers are shown in Fig. 17 and the etched ones are shown in Fig. 18.

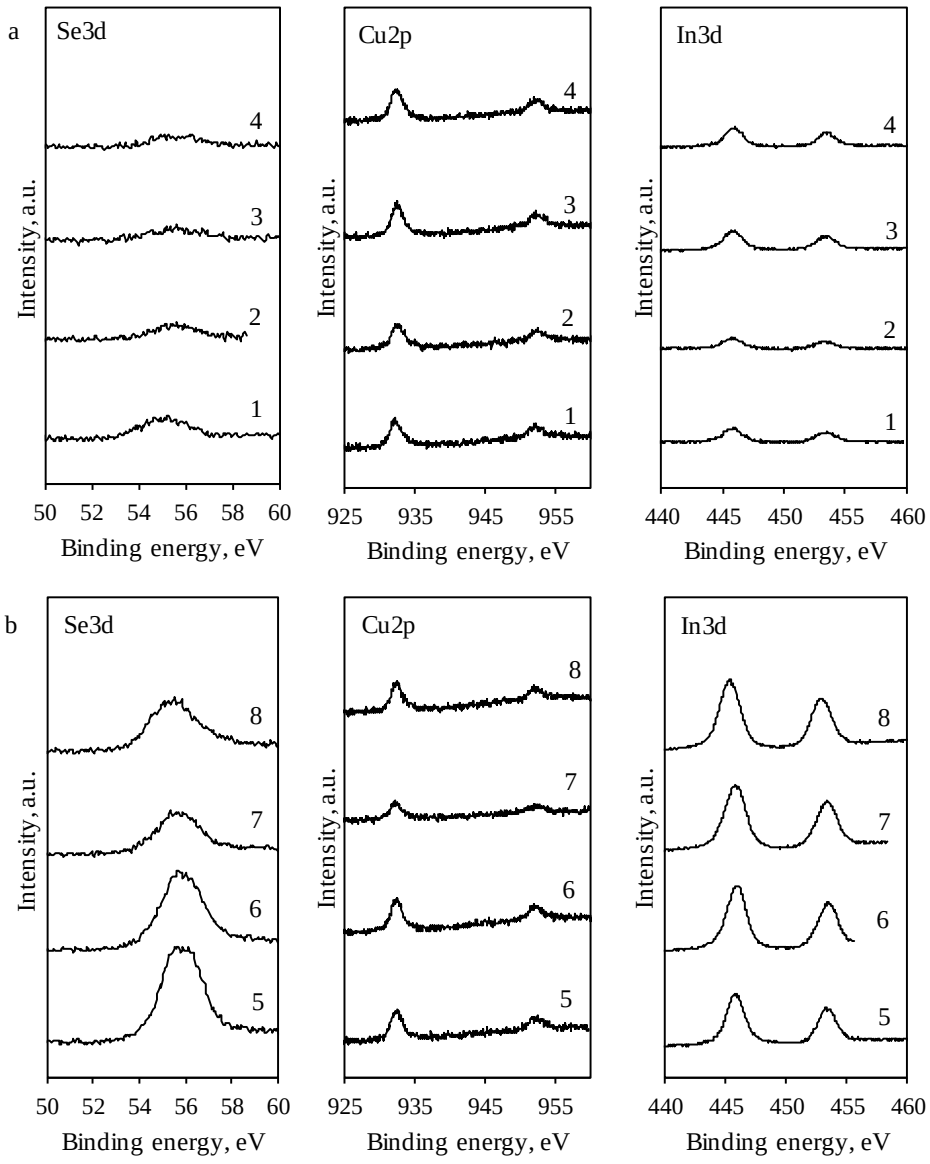

Fig. 17. High-resolution XPS spectra in $Se3d_{3/2}$ and $Se3d_{5/2}$, $Cu2p_{3/2}$ and $Cu2p_{1/2}$, $In3d_{5/2}$ and $In3d_{3/2}$ regions of copper and indium selenide layers on a glass substrate. Selenization 2 hours (a) and 3 hours (b). The temperature and duration of copper(I/II) salt solution treatment: 1, 5 – 10 min at 40°C; 2, 6 – 20 min at 40°C; 3, 7 – 5 min at 60°C; 4, 8 – 10 min at 60°C. 10 min indium(III) salt solution treatment. Layers unetched.

Samples that have been selenized for two hours (Fig. 17 (a) and Fig. 18 (a)) have significantly lower Se3d peaks, showing that selenium concentration is lower than on the samples that were selenized for three hours (Fig. 17 (b) and Fig. 18 (b)). Also, layers that have not been etched (Fig. 17) have lower peaks than their etched counterparts (Fig. 18). This is probably due to the fact that during copper(II/I) salt solution treatment and indium(III) salt solution treatment, the top layers are formed have less selenium. This is why the deeper (etched) layer contains more selenium.

All etched two-hour samples (Fig. 18 (a)) in Se3d spectra region have peaks at similar binding energy 54.6–54.8 eV (Table 7). This corresponds with the In_2Se_3 binding energy 54.8 eV [149]. The two-hour selenization samples' peak values (Fig. 18 (a) are shifted to lower binding energy compared to the three-hour ones (Fig. 18 (b)). This indicates that peaks may have shifted due to more deposited elemental selenium with higher binding energy of 55.7 eV [140]. Also, $CuInSe_2$ fits all Se3d spectra peak values with the three-hour selenization samples (Fig. 18 (b)) with the binding energy of 55.0–55.18 eV [150, 151]. The results correspond with the XRD data.

The high resolution XPS spectra in $Cu2p_{3/2}$ and $Cu2p_{1/2}$ regions are shown in Fig. 17 and Fig. 18 for not etched and for etched layers in Cu2p graphs, respectively. In case of an unetched sample, layers that were selenized for two hours (Fig. 17 (a)) and three hours (Fig. 17 (b)) have similar and rather low peaks. The same etched layers (Fig. 18) show much higher peaks compared to the unetched samples. This can be explained by the third layer formation step: more indium-containing compounds (like In_2Se_3) can be found on the top layer, more copper-containing compounds can be found deeper in the layer (like $Cu_{0.87}Se$). The top layer may be contaminated more by impurities, such as oxides and salt residues from the solutions.

All etched samples (Fig. 18) of $Cu2p_{3/2}$ spectra region have similar binding energy peaks at 932.3–932.5 eV (Table 7). This peak corresponds with a number of compounds: $CuInSe_2$ (BE=931.8–932.49 eV) [151], Cu_2Se (BE=931.9–932.5 eV) [152] and Cu_2O (BE=932.3–932.5 eV) [153, 154]. The $Cu2p_{1/2}$ spectra have peak values at 952.2–952.4 eV and it corresponds with $CuInSe_2$ (BE=932.31 eV) [151] and Cu_2O (BE=932.5 eV) [154]. Not etched samples (Fig. 17) have similar binding energy peak values 932.2–932.4 eV. This means that layers have similar composition both on the surface and in the deeper layers.

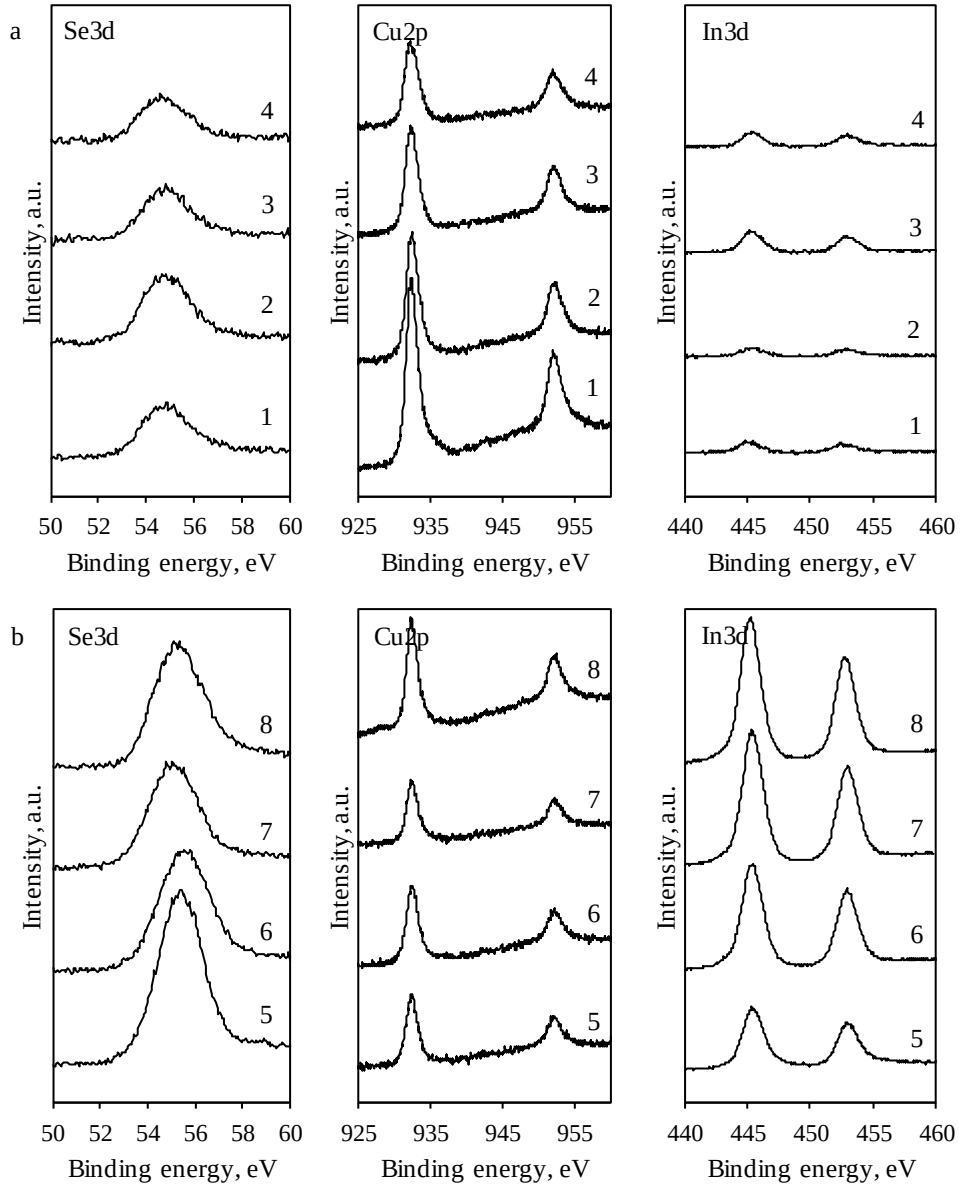

Fig. 18. High-resolution XPS spectra in $Se3d_{3/2}$ and $Se3d_{5/2}$, $Cu2p_{3/2}$ and $Cu2p_{1/2}$, $In3d_{5/2}$ and $In3d_{3/2}$ regions of obtained copper and indium selenide layers on a glass substrate. Selenization 2 hours (a) and 3 hours (b). The temperature and duration of copper(I/II) salt solution treatment: 1, 5 – 10 min at 40°C; 2, 6 – 20 min at 40°C; 3, 7 – 5 min at 60°C; 4, 8 – 10 min at 60°C. 10 min indium(III) salt solution treatment. All layers are etched.

In3d graphs in Fig. 17 show high-resolution XPS spectra in $In3d_{5/2}$ and $In3d_{3/2}$ regions of copper and indium selenide unetched layers, while Fig. 18 shows the same spectra in etched layers. Samples selenized for two hours (Fig. 17 (a) and Fig. 18 (a)) show much lower peaks than the ones that were selenized for three hours (Fig. 17 (b) and Fig. 18 (b)). Both unetched and etched layers of the two-hour selenization samples show similar peak height values, while three-hour selenization samples show slightly higher peaks in the etched layers. This indicates that indium compounds are spread rather evenly across the top and in the deeper layers. Also, the top layer may have some impurities, such as oxide or residual salts from solutions.

All etched samples (Fig. 18) in the $In3d_{5/2}$ spectra region have similar binding energy peaks at 445.1–445.5 eV (Table 7). These spectra values correspond with In_2Se_3 (BE=445.1 eV) [155]. However, samples with an unetched layer (Fig. 18) have shifted peaks to higher binding energy to 445.8–446.0 (except pattern (8)); these values correspond with $In(OH)_3$ (BE=445.0–445.2 eV) [156] and $InCl_3$ (BE=445.9 eV) [157]. This shows that there is residual indium chloride on the surface of the layers and it is not present in deeper layers.

$In3d_{3/2}$ spectra region have peaks of binding energy in the range of 452.8–453.7 eV. The closest match is $InCl_3$ (BE=454.1 eV) [155]). Similarly to $In3d_{5/2}$, spectra region, $In3d_{5/2}$ region peaks are higher on the etched samples, once again indicating there are more $InCl_3$ on the top layer compared to the deeper layers. The NIST XPS database has very few entries in the $In3d_{3/2}$ spectra region, thus the results are inconclusive.

Some impurity elements, such as O, Cl and C were also detected by XPS analysis. The impurity of O is due to the exposure to atmosphere, and hydrolysis results in Cu_2O and In_2O_3 formation, Cl is a residual element from the precursor $InCl_3$ solution, C 1s of adventitious carbon is used as reference.

Table 7. XPS spectra peak values of copper and indium selenide layers on a glass substrate. Samples were treated for 10 min in an indium(III) salt solution.

Conditions of treatment					Binding energy, eV				
					$Se3d_{5/2}$	$Cu2p_{3/2}$	$Cu2p_{1/2}$	$In3d_{5/2}$	$In3d_{3/2}$
Not etched									
Selenization	2 h	Copper(I/II) salt solution treatment	40°C	10 min	55.0	932.1	952.2	445.8	453.5
				20 min	55.6	932.5	952.4	445.8	453.5
			60°C	5 min	55.6	932.4	952.3	445.8	453.5
				10 min	55.2	932.4	952.4	445.9	453.5
	3 h		40°C	10 min	55.8	932.4	952.4	445.9	452.9
				20 min	55.8	932.3	952.3	446.0	453.5
			60°C	5 min	55.6	932.2	952.3	445.9	453.5
				10 min	55.4	932.3	952.3	445.4	453.6
Etched									
Selenization	2 h	Copper(I/II) salt solution treatment	40°C	10 min	54.7	932.4	952.2	445.1	453.7
				20 min	54.8	932.4	952.3	445.4	453.0
			60°C	5 min	54.8	932.3	952.3	445.4	453.0
				10 min	54.6	932.3	952.2	445.4	453.1
	3 h		40°C	10 min	55.3	932.4	952.3	445.5	453.1
				20 min	55.5	932.5	952.4	445.4	452.6
			60°C	5 min	55.0	932.4	952.3	445.4	453.3
				10 min	55.2	932.4	952.3	445.3	452.8
Selenization 3 h					55.6	–	–	–	–

Table 8. Atomic content of elements on the surface of copper and indium selenide layer evaluated from XPS. All layers are etched.

Conditions of treatment							Atomic content, %		
							Se	Cu	In
Indium(III) salt solution treatment	10 min	Selenization	2 h	Copper(I/II) salt solution treatment	40°C	10 min	35.27	47.56	17.17
			3 h		40°C	10 min	56.69	15.92	27.40
						20 min	41.63	17.55	40.82
					60°C	10 min	37.66	21.74	40.61
	20 min		3 h		40°C	10 min	24.92	31.01	44.07

The atomic content of elements on the surface layers are shown in Table 8. The results show concentration changes in the atomic percentage with the differing conditions during each layer formation step. The compared sample (5) was formed using these conditions: 3-hour selenization, 10 min at 40°C copper solution treatment and 10 min indium(III) salt solution treatment. Sample (1) was contained in exactly the same conditions, except selenization took 2 hours. It has a much lower selenium content (35.27%) compared to sample (5) (56.69%). Next, the copper content is compared. Sample (5) was treated in a copper solution at 40°C for 10 min and has 15.92% copper content. As expected, samples that have been treated for a longer duration (6–20 min at 40°C) and higher temperature (8–10 min at 60°C) have a higher copper content of 17.55% and 21.74%, accordingly. Finally, a 10 min (5) and 20 min (9) indium(III) salt solution treatment conditions are compared. The latter shows much higher indium content 44.07% against 27.40%

The research tried to determine the reaction pathways using XRD and XPS analysis data of copper and indium selenide layers deposited using the SILAR method. It can be seen that during the first layer formation step, red, elemental, amorphous selenium Se^0 is deposited. Next, the layer is treated with a solution containing copper(I) ions, obtaining the $Cu_{0.87}Se$ phase. When this layer was exposed to a solution containing indium(III) ions, the XRD analysis shows that $Cu_{0.87}Se$ and In_2Se_3 compounds coexist in the layer before annealing. After annealing, both XRD and XPS confirm that the following phases are present Se^0, $Cu_{0.87}Se$, In_2Se_3, $CuInSe_2$.

3.4.3. SEM/EDS analysis

Scanning electron microscopy is a convenient technique for analysing the surface microstructure of thin films. Fig. 19 shows scanning electron micrographs of copper and indium selenide layers formed on a glass substrate. Elemental maps are shown in Fig. 21 and energy-dispersive X-ray spectroscopy spectra are presented in Fig. 22.

A scanning electron microscope was used for studying the surface morphology and the micro structural features of copper and indium selenide layers on glass. SEM micrographs are shown at 1000 and 4000 magnifications, respectively. Looking at SEM micrographs we can see that the sample that was selenized for 2 hours (Fig. 19 (a)) looks more uniform compared to 3-hour samples (Fig. 19 (b), (c), (d)). Also, the micrograph of the 2-hour selenization sample (Fig. 19 (a)) shows a compact structure composed of single type grains. Though the grains are small they are densely packed in clusters. The individual grains are well-defined, spherical and similar in size, about 0.5–1.0 μm. In all 3-hour selenization samples (Fig. 19 (b), (c), (d)) gains exist in an agglomerated, dendritic structures and individual the grains are undefined.

SEM top and side images of copper and indium selenide layers were acquired to assess the thickness of the layer (shown in Fig. 20). The thickness of an obtained layer mostly depends on the initial selenium deposition duration. The inset reveals the layer size to be around 26 μm for 2-hour selenized samples and around 90 μm for 3-hour selenized samples. Different copper(I/II) and indium(I/II) salt solution treatment conditions do not seem to have any significant impact on the thickness of the formed layers.

Energy dispersive X-ray spectroscopy (EDS) analysis was performed on the obtained layers (Fig. 22). Besides the main elements of Se, Cu and In, several other elements were found: O, Mg, Si, S, Cl, Na, Ca, S. O can be attributed to the adsorbed oxygen from atmosphere in the dendritic layer structure. Si and Mg could be found in the glass substrate. Remaining Na, S and Cl may be adsorbed residue from different solutions during layer formation steps.

Peaks correspond with the atomic mass ratios on the layer. The sample in Fig. 22 (d) was selenized for 3 hours, treated with copper solution for 10 min at 60°C, treated with indium solution for 20 min. The sample in Fig. 22 (a) was obtained using the same conditions, except selenization took 2 hours. As expected, the 3-hour selenization sample has a much higher Se peak. The elemental map also confirms these results: the 2-hour selenization sample (Fig. 21 (a)) has very little red area that corresponds to selenium compared to the 3-hour selenization sample (Fig. 21 (d)).

Next, the previous layer (Fig. 22 (d)) is compared to the layer that has a lower copper solution treatment temperature (40°C) (Fig. 22 (b)). It has a much lower Cu peak, indicating that copper-rich layers obtained using a higher (60°C) temperature.

The elemental map (Fig. 21 (b)) shows almost no light-green areas that correspond to copper as compared to Fig. 21 (d).

Finally, energy dispersive X-ray analysis results look very similar for both 10 min (Fig. 22 (c)) and 20 min (Fig. 22 (d)) indium treatment layers. Similar results can be seen on elemental maps (Fig. 21 (c) and Fig. 21 (d)); small areas contain dark-green colour that corresponds with indium. This data correlates with XDS and XPS analyses.

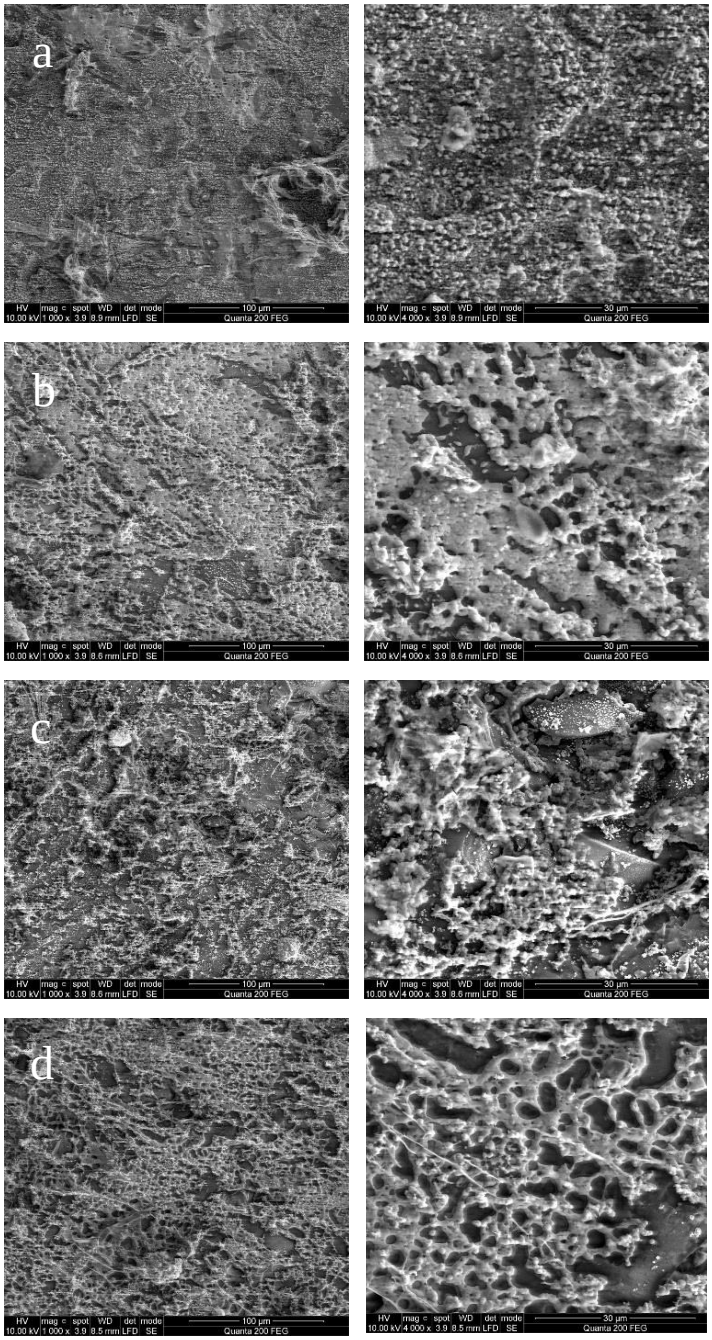

Fig. 19. SEM images of copper and indium selenide layer on a glass substrate. Samples were selenized: (a) – 2 hours and (b), (c), (d) – 3 hours. The temperature and duration of copper(I/II) salt solution treatment: (b) – 10 min at 40°C; (a), (c), (d) – 10 min at 60°C. Indium(III) salt solution treatment: (c) – 10 min; (a), (b), (d) – 20 min. All samples were annealed.

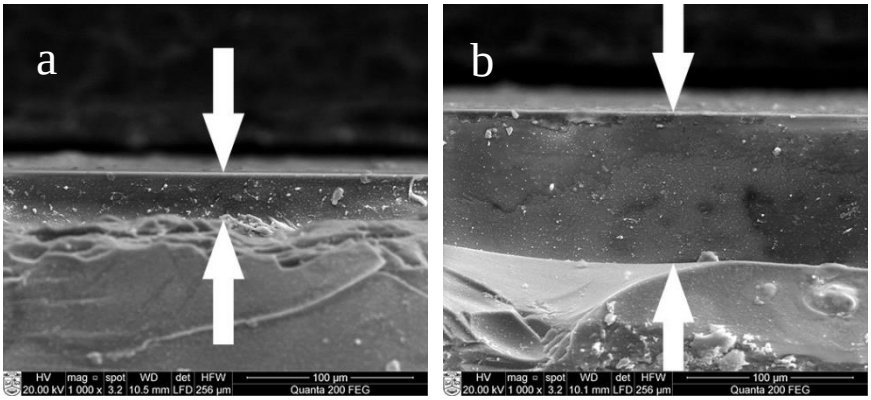

Fig. 20. SEM side images of copper and indium selenide layer on a glass substrate. Samples were selenized: (a) – 2 hours and (b) – 3 hours. The temperature and duration of copper(I/II) salt solution treatment: 10 min at 60°C. Indium(III) salt solution treatment: 20 min. All samples were annealed.

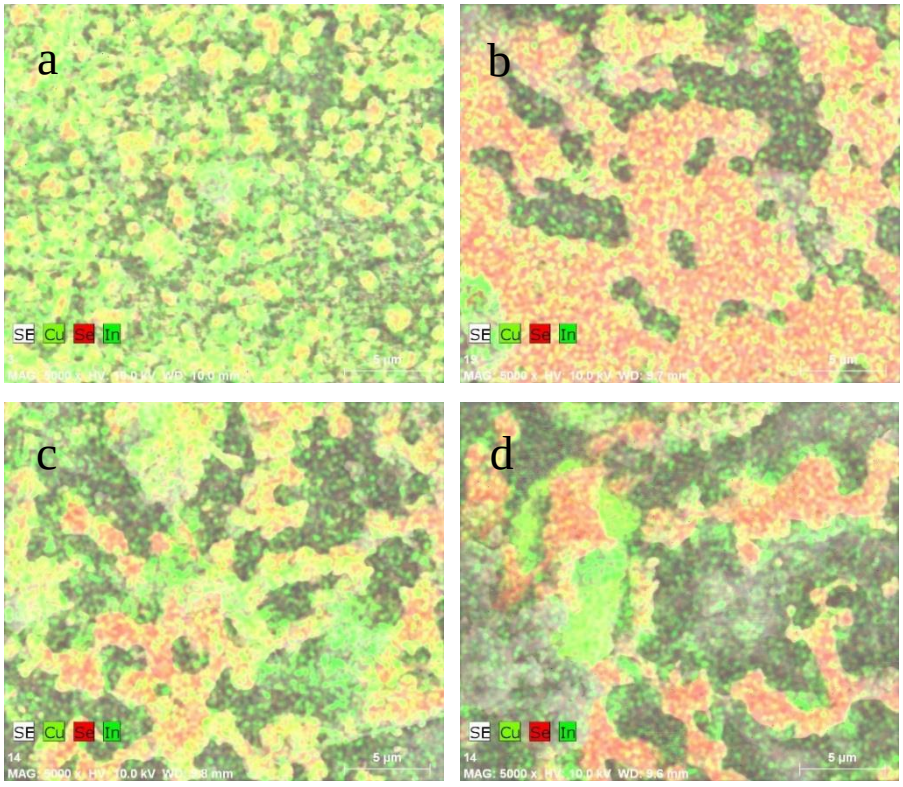

Fig. 21. Elemental map images of copper and indium selenide layer on a glass substrate. Samples were selenized: (a) – 2 hours and (b), (c), (d) – 3 hours. The temperature and duration of copper(I/II) salt solution treatment: (b) – 10 min at 40°C; (a), (c), (d) – 10 min at 60°C. Indium(III) salt solution treatment: (c) – 10 min; (a), (b), (d) – 20 min. All samples were annealed.

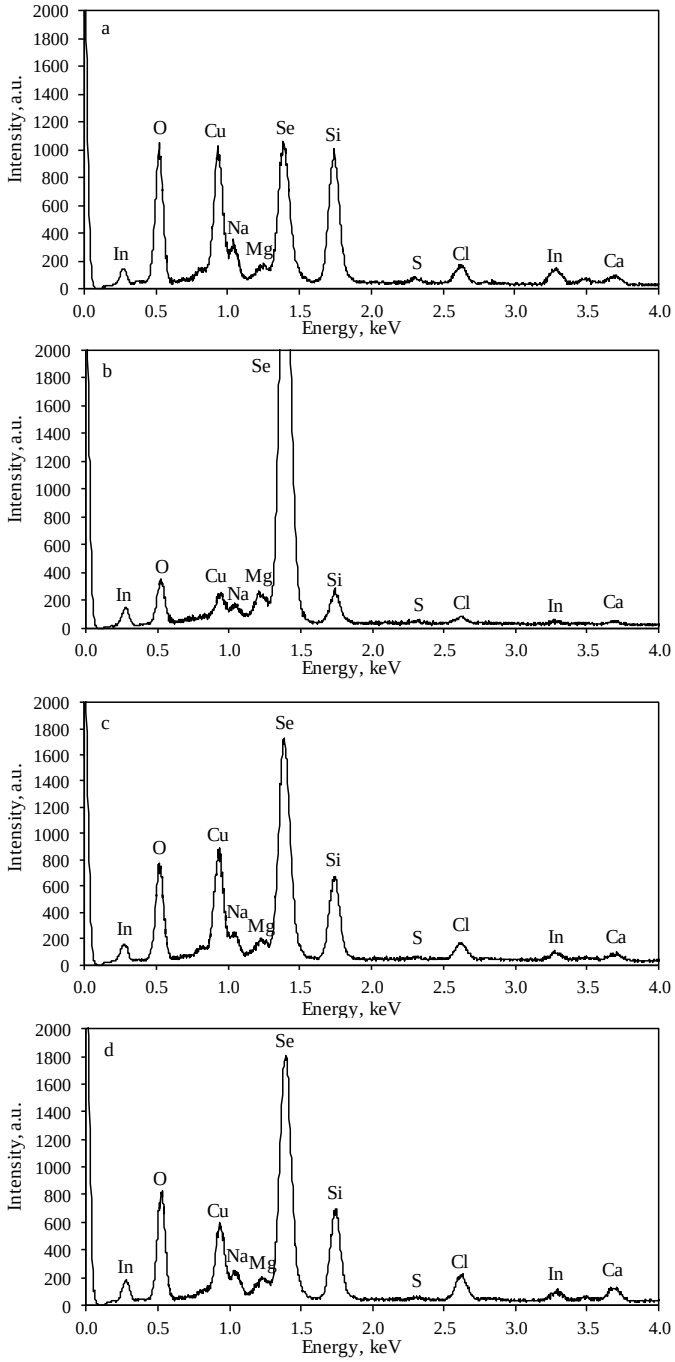

Fig. 22. EDS images of copper and indium selenide layer on a glass substrate. Samples were selenized: (a) – 2 hours and (b), (c), (d) – 3 hours. The temperature and duration of copper(I/II) salt solution treatment: (b) – 10 min at 40°C; (a), (c), (d) – 10 min at 60°C. Indium(III) salt solution treatment: (c) – 10 min at 40°C; (a), (b), (d) – 20 min at 40°C. All samples were annealed.

3.4.4. AAS analysis

Atomic absorption spectroscopy analysis method was used to determine the amount of selenium, copper and indium which are shown in Table 9. Data here mostly coincide with the data obtained by using other analysis methods.

Samples which are submerged into a mixture of solutions H_2SeO_3 and $KHSO_3$ for longer durations deposit more selenium. The same can be said about copper(I/II) salt solution treatment: higher temperatures and longer durations result in copper-rich layers. Selenium and copper data is discussed in the discussions of copper selenide layers AAS analysis on p.45.

The durations of indium(III) salt solution treatment seem to have the same effect as depositing selenium layer from a mixture of solutions H_2SeO_3 and $KHSO_3$ durations, as well as copper(I/II) salt solution treatment durations. Longer treatment in indium(III) salt solution will provide indium-rich layer samples. Layers that have been treated for 10 min have 0.218–0.244 μmol/cm^2, and 20 min samples have 0.233–0.366 μmol/cm^2 of indium.

One more observation that can be made from AAS analysis data is that the amount of copper is lower (0.368–0.808 μmol/cm^2) on samples after indium(III) salt solution treatment compared to before the treatment (0.787–1.028 μmol/cm^2). This may be due to the reaction between copper selenide and indium(III) ions, as noted in XRD discussions and in equations (51) and (52):

Table 9. Calculated elemental amount to area units for selenium, copper, indium in copper and indium selenide layers on glass

Conditions of treatment							Amount of elements, μmol/cm^2		
							Se	Cu	In
Indium(III) salt solution treatment	10 min	Selenization	2 h	Copper(I/II) salt solution treatment	40°C	10 min	1.165	0.368	0.218
						20 min	1.203	0.520	0.229
					60°C	5 min	1.197	0.537	0.231
						10 min	1.199	0.720	0.244
			3 h		40°C	10 min	2.835	0.530	0.227
						20 min	2.949	0.615	0.237
					60°C	5 min	2.797	0.723	0.238
						10 min	2.886	0.808	0.241
	20 min		2 h		40°C	10 min	1.218	0.348	0.233
						20 min	1.196	0.487	0.244
					60°C	5 min	1.208	0.503	0.273
						10 min	1.228	0.687	0.278
			3 h		40°C	10 min	2.861	0.502	0.237
						20 min	2.848	0.587	0.273
					60°C	5 min	2.949	0.690	0.294
						10 min	2.886	0.775	0.366

3.4.5. Optical properties

Tauc plot was used to calculate the optical band gap of formed layers. The plot shows the energy of the light hv on the abscissa axis and the absorption quantity $(\alpha hv)^n$ on the ordinate axis, where α is the absorption coefficient of the studied layer materials. The resulting plot has a distinct linear regime, when $n = 2$, indicating a direct band gap transition. It denotes the onset of absorption. Extrapolating the linear region to the abscissa yields the energy of the optical band gap of the material.

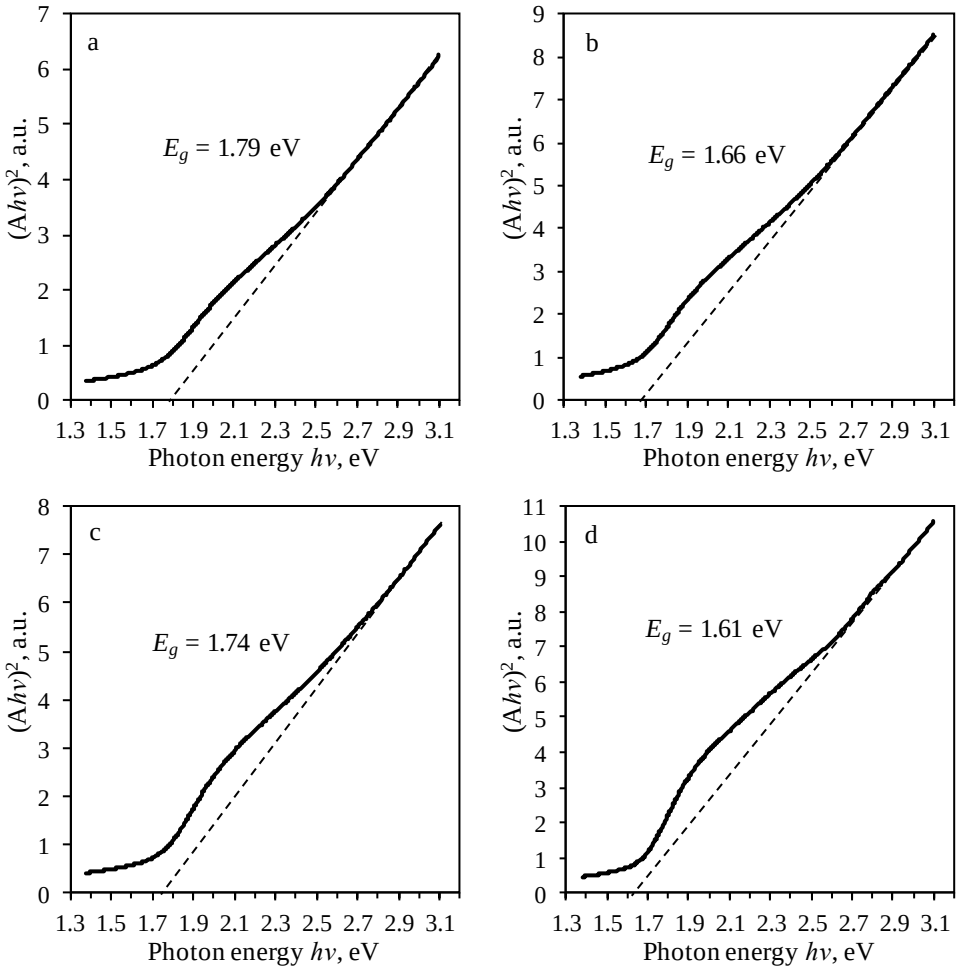

Fig. 23. A plot of $(Ahv)^2$ versus hv of multiphase copper and indium selenide layer. Selenization 2 hours (a), (c) and 3 hours (b), (d). Copper(I/II) salt solution treatment at 40°C for 20 min (a), (b), (c), (d). Indium(III) salt solution treatment 10 min (a), (b) and 20 min (c), (d).

Calculated $(Ahv)^2$ versus hv graphs have a linear part. Band gap E_g values were calculated (Table 11). Band gap values of the semi-conductors of the formed layers

found in literature are provided in Table 10. The measured band gap values are between 1.60–1.87 eV. This equates to the absorption start at 663–775 nm. These values fall under the most of compounds' band gap values that were identified using XRD (Table 6) and XPS. Direct band gap values found in literature are shown in Table 10.

Samples that have been selenized for 2 hours and treated in an indium solution for 10 minutes (1–4, Table 11) have a higher band gap value (1.78–1.87 eV) compared to the samples that have been selenized for 3 hours (5–8, Table 11) (1.62–1.76 eV). The lower band gap values for 3-hour selenization samples indicate that they may contain more elemental selenium phase because they are shifted towards elemental selenium band gap of 1.60 eV which is found in literature [158]. Two-hour samples have band gaps shifted, higher values that correspond to $Cu_{0.87}Se$ (1.67–1.81 eV) and In_2Se_3 (1.70 eV) bandgaps [159, 160]. Similar results can be seen for samples that have been treated for 20 minutes in indium solution, two-hour samples (9–12, Table 11) have higher band gaps compared to three-hour ones (13–16, Table 11), also, indicating more elemental selenium in the latter ones. The results coincide with XRD data in Fig. 15 and Fig. 16. Selenization time has the biggest impact on the band gap values of the formed layers.

Also, according to the XRD data, two-hour selenization samples (Fig. 15, 1–4) have more $Cu_{0.87}Se$ phase compared to two-hour selenization samples (Fig. 15, 5–8), thus they have higher band gap values.

Different temperatures and treatment durations of copper(I/II) salt solution treatment do not seem to have significant impact on the band gap.

Similar can be said about indium(III) salt solution treatment. Although the layers that have been treated for 10 min in indium(III) salt solution (1–8, Table 11) tend to have slightly higher band gap (1.62–1.87 eV) compared to 20 min ones (9–16, Table 11) (1.60–1.74 eV). This means that more In_2Se_3 were formed due to longer indium(III) salt solution treatment. This also coincides with the XRD data in Fig. 15 and Fig. 16. With longer indium(III) salt solution treatment times, slightly more In_2Se_3 is obtained (and less $Cu_{0.87}Se$), thus it has slightly higher band gap values.

Table 10. Semiconductor values

Semiconductor	Band gap E_g, eV	Literature
Se	1.60	[158]
$Cu_{0.87}Se$	1.67–1.81	[160]
In_2Se_3	1.70	[159]
$CuInSe_2$	1.04	[70]

Table 11. Calculated band gap E_g values for the obtained samples. Samples were selenized: 1–4, 9–12 – 2 hours and 5–8, 13–16 – 3 hours. The temperature and duration of copper(I/II) salt solution treatment: 1, 5, 9, 13 – 10 min at 40°C; 2, 6, 10, 14 – 20 min at 40°C; 3, 7, 11, 15 – 5 min at 60°C; 4, 8, 12, 16 – 10 min at 60°C. Indium(III) salt solution treatment: 1–8 – 10 min at 40°C; 9–16 – 20 min at 40°C. All samples were annealed.

Conditions of treatment							Sample	Band gap E_g, eV
Indium(III) salt solution treatment	10 min	Selenization	2 h	Copper(I/II) salt solution treatment	40°C	10 min	1	1.78
						20 min	2	1.79
					60°C	5 min	3	1.87
						10 min	4	1.84
			3 h		40°C	10 min	5	1.76
						20 min	6	1.66
					60°C	5 min	7	1.65
						10 min	8	1.62
	20 min		2 h		40°C	10 min	9	1.66
						20 min	10	1.74
					60°C	5 min	11	1.68
						10 min	12	1.71
			3 h		40°C	10 min	13	1.62
						20 min	14	1.61
					60°C	5 min	15	1.64
						10 min	16	1.60

CONCLUSIONS

1. Using simple methods, $H_2Se_nS_2O_6$-type acids are formed. Upon analysing acids using three methods, it was determined that *n* varies between 1.04 and 2.1. The formation and decomposition of selenopolythionates was studied and it was determined that these processes depend greatly on the concentration, temperature and additives. Using $KHSO_3$ instead of H_2SO_3 allows increasing the concentration of selenotrithionate and diselenotetrathionate acid solution to 0.2 mol/l and its stability, as H_2SO_4 was eliminated.

2. Selenium, copper selenide, copper and indium selenide layers were obtained through successive ionic layer adsorption and reaction (SILAR) method using $H_2Se_nS_2O_6$ as a selenium precursor.

3. Multiple phases were identified using XRD analysis method: monoclinic selenium, hexagonal klockmannite $Cu_{0.87}Se$, cubic berzelianite $Cu_{2-x}Se$, tetragonal umangite Cu_3Se_2, cubic copper selenide Cu_7Se_4, cubic indium selenide In_2Se_3. Copper selenide peaks are most dominant with hexagonal klockmannite phase. New intense hexagonal selenium, more intense indium selenide In_2Se_3 and new cubic copper indium selenide $CuInSe_2$ phases are observed after annealing in an inert nitrogen atmosphere.

4. Copper and indium selenide layers can be formed using a three-step method:
   - Selenium layer (step 1);
   - $Cu_{0.87}Se$, $Cu_{2-x}Se$ (step 2);
   - In_2Se_3, $Cu_{0.87}Se$, Cu_3Se_2, Cu_7Se_4 (step 3);
   - $CuInSe_2$, In_2Se_3, $Cu_{0.87}Se$, Se (after annealing in an inert nitrogen atmosphere).

5. XPS analysis confirms that multiphase layers are formed containing $CuInSe_2$, In_2Se_3, $In(OH)_3$, Cu_2Se, Cu_2O and elemental selenium. Also, adsorbed $InCl_3$ can be found on the surface of the layer.

6. SEM analysis shows that layers that were selenized for two hours are grainy, more uniform compared to three hours. EDS analysis shows that layers that were selenized for longer contain more selenium and samples that were treated with copper solution in higher temperature (60°C) have more copper compared to the ones treated in lower temperature (40°C).

7. Optical analysis showed that direct band gap values are between 1.60 and 1.87 eV. Obtained layers are multiphase and their optical properties are characteristic to the optical properties of copper and indium selenide.

ACKNOWLEDGEMENTS

First and foremost, I would like to express my greatest gratitude to my supervisor prof. Ingrida Ancutienė for the dedication and commitment in helping me to write the most significant academic paper. Without her guidance, devotion and academic expertise my study would not have been completed.

I would like to thank: Antanas Baltušnikas for recording the XRD spectra, Rimantas Gudaitis for taking the SEM pictures, Vitalija Jasulaitienė for recording the XPS spectra, and Remigijus Ivanauskas for helping me record the AAS analysis data. Also, I would like to thank my colleague Linas Samardokas who cheered me up and motivated me to keep working. Special thanks go to Judita Šukytė for working together long hours in the lab, for help in the discussion and results summarization of selenopolythionate acids study.

And last but not least, thanks go to family: my parents Remigijus Ivanauskas and Tamara Ivanauskienė and my dear sister Eglė Ivanauskaitė for warmest encouragement, support and motivation not just during the process of writing the thesis, but during my whole life.

LIST OF REFERENCES

1. STEVELS, A.L.N. and JELLINEK, F. Phase transitions in copper chalcogenides: I. The copper-selenium system. *Recueil des Travaux Chimiques des Pays-Bas*. 2010. Vol. 90, no. 3, p. 273–283.

2. DOMASHEVSKAYA, E.P., GORBACHEV, V.V., TEREKHOV, V.A., KASHKAROV, V.M., PANFILOVA, E.V. and SHCHUKAREV, A.V. XPS and XES emission investigations of d–p resonance in some copper chalcogenides. *Journal of Electron Spectroscopy and Related Phenomena*. 2001. Vol. 114–116, p. 901–908.

3. XIAO, X.X., XIE, W.J., TANG, X.F. and ZHANG, Q.J. Phase transition and high temperature thermoelectric properties of copper selenide $Cu_{2-x}Se$ ($0 \leq x \leq 0.25$). *Chinese Physics B*. 2011. Vol. 20, no. 8, p. 87201.

4. LÉVY-CLÉMENT, C., NEUMANN-SPALLART, M., HARAM, S.K. and SANTHANAM, K.S.V. Chemical bath deposition of cubic copper (I) selenide and its room temperature transformation to the orthorhombic phase. *Thin Solid Films*. 1997. Vol. 302, no. 1–2, p. 12–16.

5. NANCHEVA, N., DOCHEVA, P., DJOURELOV, N. and BALCHEVA, M. *Positron and X-ray diffraction study of Cu–Se, In–Se and $CuInSe_2$ thin films*. 2002.

6. SU, H.L., XIE, Y., QIAO, Z. and QIAN, Y.T. Formation of $Cu_{2-x}Se(en)_2$ in a solvothermal process and conversion to nanocrystalline $Cu_{2-x}Se$. *Materials Research Bulletin*. 2000. Vol. 35, no. 7, p. 1129–1135.

7. OHTANI, T., TACHIBANA, Y., OGURA, J., MIYAKE, T., OKADA, Y. and YOKOTA, Y. Physical properties and phase transitions of β $Cu_{2-x}Se$ ($0.20 \leq x \leq 0.25$). *Journal of Alloys and Compounds*. 1998. Vol. 279, no. 2, p. 136–141.

8. LAKSHMI, M, BINDU, K, BINI, S, VIJAYAKUMAR, K.P, KARTHA, C.Sudha, ABE, T and KASHIWABA, Y. Reversible $Cu_{2-x}Se \leftrightarrow Cu_3Se_2$ phase transformation in copper selenide thin films prepared by chemical bath deposition. *Thin Solid Films*. 2001. Vol. 386, no. 1, p. 127–132.

9. HERMANN, A.M. and FABICK, L. Research on polycrystalline thin-film photovoltaic devices. *Journal of Crystal Growth*. 1983. Vol. 61, no. 3, p. 658–664.

10. IVANAUSKAS, R. and JANICKIS, V. Formation of copper selenide layers on the surface of polyamide films by the use of potassium selenotrithionate. *Polish Journal of chemistry*. 2008. Vol. 82, no. January, p. 2281–2292.

11. MANE, R.S. and LOKHANDE, C.D. Chemical deposition method for metal chalcogenide thin films. *Materials Chemistry and Physics*. 2000. Vol. 65,

no. 1, p. 1–31.

12. KORZHUEV, M. A. Dufour effect in superionic copper selenide. *Physics of the Solid State*. 1998. Vol. 40, no. 2, p. 217–219.

13. LIN, Z., HOLLAR, C., KANG, J., YIN, A., WANG, Y., SHIU, H., HUANG, Y., HU, Y., ZHANG, Y. and DUAN, X. A Solution Processable High-Performance Thermoelectric Copper Selenide Thin Film. *Advanced Materials*. 2017. Vol. 29, no. 21, p. 1606662.

14. SANDOVAL-PAZ, M. G., RODRIGUEZ, C. A., PORCILE-SAAVEDRA, P. F. and TREJO-CRUZ, C. Study of the crystallographic phase change on copper (I) selenide thin films prepared through chemical bath deposition by varying the pH of the solution. *Journal of Solid State Chemistry*. 2016. Vol. 239, p. 106–112.

15. GOSAVI, S.R., DESHPANDE, N.G., GUDAGE, Y.G. and SHARMA, Ramphal. Physical, optical and electrical properties of copper selenide (CuSe) thin films deposited by solution growth technique at room temperature. *Journal of Alloys and Compounds*. 2008. Vol. 448, no. 1, p. 344–348.

16. About - Electrochemical Products, Inc. [online]. [Accessed 12 May 2017]. Available from: https://www.epi.com/about/

17. PAZHAMALAI, P., KRISHNAMOORTHY, K. and KIM, S. Hierarchical copper selenide nanoneedles grown on copper foil as a binder free electrode for supercapacitors. *International Journal of Hydrogen Energy*. 2016. Vol. 41, no. 33, p. 14830–14835.

18. HESSEL, C.M., PATTANI, V.P., RASCH, M., PANTHANI, M.G., KOO, B., TUNNELL, J.W. and KORGEL, B.A. Copper Selenide Nanocrystals for Photothermal Therapy. *Nano Letters*. 2011. Vol. 11, no. 6, p. 2560–2566.

19. OHTANI, T., MOTOKI, M., KOH, K. and OHSHIMA, K. Synthesis of binary copper chalcogenides by mechanical alloying. *Materials Research Bulletin*. 1995. Vol. 30, no. 12, p. 1495–1504.

20. ЧИЖИКОВ, Д.М. and СЧАСТЛИВЫЙ, В.П. *Селен и селениды*. Москва, 1964.

21. ОБОЛОНЧИК, В.А. *Селениды*. Москва, 1972.

22. SU, H., XIE, Y., LI, B. and QIAN, Y. A simple, convenient, mild hydrothermal route to nanocrystalline CuSe and Ag_2Se. *Materials Research Bulletin*. 2000. Vol. 35, no. 3, p. 465–469. DOI 10.1016/S0025-5408(00)00233-6.

23. HAN, Z.H., LI, Y.P., ZHAO, H.Q., YU, S.H., YIN, X.L. and QIAN, Y.T. A simple solvothermal route to copper chalcogenides. *Materials Letters*. 2000. Vol. 44, no. 6, p. 366–369.

24. LIPPKOW, D. and STREHBLOW, H.H. Structural investigations of thin films of copper–selenide electrodeposited at elevated temperatures. *Electrochimica Acta*. 1998. Vol. 43, no. 14, p. 2131–2140.

25. ROQUET, L., BELGSIR, E.M., LÉGER, J.M. and LAMY, C. Kinetics and mechanisms of the electrocatalytic oxidation of glycerol as investigated by chromatographic analysis of the reaction products: Potential and pH effects. *Electrochimica Acta*. 1994. Vol. 39, no. 16, p. 2387–2394.

26. ESTRADA, C.A., NAIR, P.K., NAIR, M.T.S., ZINGARO, R.A. and MEYERS, E.A. Chemical Bath Deposition of ZnSe and CuSe Thin Films Using N,N-Dimethylselenourea. *Journal of The Electrochemical Society*. 1994. Vol. 141, no. 3, p. 802.

27. MONDAL, A. and PRAMANIK, P. A solution growth technique for the preparation of copper (II) selenide thin films. *Journal of Solid State Chemistry*. 1983. Vol. 47, no. 1, p. 81–83.

28. MONDAL, A. and PRAMANIK, P. Effect of bath parameters on chemically deposited thin films of CuSe. *Journal of Solid State Chemistry*. 1984. Vol. 55, no. 1, p. 116–119.

29. PADAM, G.K. The properties of chemically deposited $Cu_{2-x}Se$ thin films. *Thin Solid Films*. 1987. Vol. 150, no. 1, p. 89–92.

30. ANDRADE, E., GARCÍA, V.M., NAIR, P.K., NAIR, M.T.S., ZAVALA, E.P., HUERTA, L. and ROCHA, M.F. Ion beam analysis of copper selenide thin films prepared by chemical bath deposition. *Nuclear Instruments and Methods in Physics Research Section B: Beam Interactions with Materials and Atoms*. 2000. Vol. 161, p. 635–640.

31. PEJOVA, Biljana and GROZDANOV, Ivan. Chemical Deposition and Characterization of Cu_3Se_2 and CuSe Thin Films. *Journal of Solid State Chemistry*. 2001. Vol. 158, no. 1, p. 49–54.

32. XIE, Y., ZHENG, X., JIANG, X., LU, J. and ZHU, L. Sonochemical Synthesis and Mechanistic Study of Copper Selenides $Cu_{2-x}Se$, β-CuSe, and Cu_3Se_2. *Inorganic Chemistry*. 2001. Vol. 41, no. 2, p. 387–392.

33. XU, S., WANG, H., ZHU, J.J. and CHEN, H.Y. Sonochemical synthesis of copper selenides nanocrystals with different phases. *Journal of Crystal Growth*. 2002. Vol. 234, no. 1, p. 263–266.

34. OHTANI, T., NONAKA, T. and ARAKI, M. Sonochemical Synthesis of Copper and Silver Chalcogenides. *Journal of Solid State Chemistry*. 1998. Vol. 138, no. 1, p. 131–134.

35. LI, H.L., ZHU, Y.C., AVIVI, S., PALCHIK, O., XIONG, J., KOLTYPIN, Y., PALCHIK, V., GEDANKEN, A. and QIAN, Y.T. Sonochemical process for

the preparation of α-CuSe nanocrystals and flakes. *J. Mater. Chem.* 2002. Vol. 12, no. 12, p. 3723–3727.

36. QIAO, Z., XIE, Y., XU, J., LIU, X., ZHU, Y. and QIAN, Y. Synthesis of nanocrystalline $Cu_{2-x}Se$ at room temperature by γ-irradiation. *Canadian Journal of Chemistry*. 2000. Vol. 78, no. 9, p. 1143–1146.

37. YAN, Y., QIAN, X., XU, H., YIN, J. and ZHU, Z. A novel solid–liquid route for the preparation of Cu_3Se_2 and Ag_2Se nanocrystals. *Inorganic Chemistry Communications*. 2003. Vol. 6, no. 1, p. 34–37.

38. ZHU, J., PALCHIK, O., CHEN, S. and GEDANKEN, A. Microwave Assisted Preparation of CdSe, PbSe, and Cu2−xSe Nanoparticles. *The Journal of Physical Chemistry B*. 2000. Vol. 104, no. 31, p. 7344–7347.

39. CARBONNELLE, P. and LAMBERTS, L. Electrochemical study of the copper-selenium system using carbon paste electrode. *Electrochimica Acta*. 1992. Vol. 37, no. 8, p. 1321–1325.

40. NOZAKI, H., SHIBATA, K., ONODA, M., YUKINO, K. and ISHII, M. Phase transition of copper selenide studied by powder X-ray diffractometry. *Materials Research Bulletin*. 1994. Vol. 29, no. 2, p. 203–211.

41. STØLEN, S., FJELLVÅG, H., GRØNVOLD, F., SIPOWSKA, J. and WESTRUM, F.E. Heat capacity, structural and thermodynamic properties of synthetic klockmannite CuSe at temperatures from 5 K to 652.7 K. Enthalpy of decomposition. *The Journal of Chemical Thermodynamics*. 1996. Vol. 28, no. 7, p. 753–766.

42. PEIRIS, S.M., PEARSON, T.T. and HEINZ, D.L. Compression of klockmannite, CuSe. *The Journal of Chemical Physics*. 1998. Vol. 109, p. 634.

43. CABRI, L.J. and KAIMAN, S. *The Canadian mineralogist*. Mineralogical Association of Canada, 1970.

44. CUNEY, M. Evolution of Uranium Fractionation Processes through Time: Driving the Secular Variation of Uranium Deposit Types. *Economic Geology*. 2010. Vol. 105, no. 3, p. 553–569.

45. Athabascaite Mineral Data. [online]. [Accessed 28 February 2017]. Available from: http://webmineral.com/data/Athabascaite.shtml

46. Bellidoite Mineral Data. [online]. [Accessed 28 February 2017]. Available from: http://webmineral.com/data/Bellidoite.shtml

47. Berzelianite Mineral Data. [online]. [Accessed 28 February 2017]. Available from: http://webmineral.com/data/Berzelianite.shtml

48. Klockmannite Mineral Data. [online]. [Accessed 28 February 2017]. Available from: http://webmineral.com/data/Klockmannite.shtml

49. Krutaite Mineral Data. [online]. [Accessed 28 February 2017]. Available from: http://webmineral.com/data/Krutaite.shtml

50. Umangite Mineral Data. [online]. [Accessed 28 February 2017]. Available from: http://webmineral.com/data/Umangite.shtml

51. GROOT, C.H. and MOODERA, J.S. Growth and characterization of a novel In_2Se_3 structure. *Journal of Applied Physics*. 2001. Vol. 89, no. 8, p. 4336–4340.

52. YANG, S., WANG, H., FU, W. and KELLEY, D.F. The synthesis and optical properties of GaSe/InSe core/shell nanoparticles. *Journal of Photochemistry and Photobiology A: Chemistry*. 2007. Vol. 192, no. 2, p. 159–165.

53. MUTLU, I.H., ZARBALIYEV, M.Z. and ASLAN, F. Indium selenide thin film preparation by sol–gel technique. *Journal of Sol-Gel Science and Technology*. 2007. Vol. 43, no. 2, p. 223–226.

54. EMZIANE, M. and NY, R.L. Crystallization of In_2Se_3 semiconductor thin films by post-deposition heat treatment. Thickness and substrate effects. *Journal of Physics D: Applied Physics*. 1999. Vol. 32, no. 12, p. 1319–1328.

55. YUDASAKA, M., MATSUOKA, T. and NAKANISHI, K. Indium selenide film formation by the double-source evaporation of indium and selenium. *Thin Solid Films*. 1987. Vol. 146, no. 1, p. 65–73.

56. JULIEN, C., KHELFA, A., BENRAMDANE, N. and GUESDON, J. P. Transport properties of InSe x flash evaporated thin films. *Journal of Materials Science*. 1995. Vol. 30, no. 19, p. 4890–4895.

57. MARSILAC, S., BERNÉDE, J.C. and CONAN, A. Change in the type of majority carriers in disordered In_xSe_{100-x} thin-film alloys. *Journal of Materials Science*. 1996. Vol. 31, p. 581–587.

58. KOHARA, N., NEGAMI, T., NISHITANI, M. and WADA, T. Preparation of Device-Quality $Cu(In,Ga)Se_2$ Thin Films Deposited by Coevaporation with Composition Monitor. *Japanese Journal of Applied Physics*. 1995. Vol. 34, no. 9, p. 1141–1144.

59. HAN, G., CHEN, Z.G., SUN, C., YANG, L., CHENG, L., LI, Z., LU, W., GIBBS, Z.M., SNYDER, G.J., JACK, K., DRENNAN, J. and ZOU, J. A new crystal: layer-structured rhombohedral In_3Se_4. *CrystEngComm*. 2014. Vol. 16, no. 3, p. 393–398.

60. YE, J., SOEDA, S., NAKAMURA, Y. and NITTONO, O. Crystal Structures and Phase Transformation in In_2Se_3 Compound Semiconductor. *Japanese Journal of Applied Physics*. 1998. Vol. 37, no. 8, p. 4264–4271.

61. TSAMOURTZI, K., SONG, J.H., BAKAS, T., FREEMAN, A.J., TRIKALITIS, P.N. and KANATZIDIS, M.G. Straightforward Route to the

Adamantane Clusters $[Sn_4Q_{10}]^{4-}$ and Use in the Assembly of Open-Framework Chalcogenides $(Me_4N)_2M[Sn_4Se_{10}]$. *Inorganic Chemistry*. 2008. Vol. 47, no. 24, p. 11920–11929.

62. WANG, C., BU, X., ZHENG, N. and FENG, P. A 3D Open–Framework Indium Telluride and Its Selenide and Sulfide Analogues. *Angewandte Chemie International Edition*. 2002. Vol. 41, no. 11, p. 1959.

63. PATHAN, H.M., KULKARNI, S.S., MANE, R.S. and LOKHANDE, C.D. Preparation and characterization of indium selenide thin films from a chemical route. *Materials Chemistry and Physics*. 2005. Vol. 93, no. 1, p. 16–20.

64. YANG, S. and KELLEY, D.F. The Spectroscopy of InSe Nanoparticles. *The Journal of Physical Chemistry B*. 2005. Vol. 109, no. 26, p. 12701–12709.

65. BANSODE, S.B., KAPADNIS, R.S., ANSARI, A.S., WAGH, V.G., KULKARNI, A.N., KALE, S.S. and PATHAN, H.M. Indium selenide microrod films: chemical bath deposition from acidic bath. *Journal of Materials Science: Materials in Electronics*. 2016. Vol. 27, no. 12, p. 12351–12356.

66. PANDA, B. *Structural and electronic properties of chalcopyrite semiconductors*. National Institute Of Technology, 2011.

67. Thin film solar (photovoltaic) cell. [online]. [Accessed 14 July 2016]. Available from: http://www.daviddarling.info/encyclopedia/T/AE_thin_film_cell.html

68. GORLEY, P.M., KHOMYAK, V.V., VOROBIEV, Y.V., GONZÁLEZ, J., HORLEY, P.P. and GALOCHKINA, O.O. Electron properties of n- and p-$CuInSe_2$. *Solar Energy*. 2008. Vol. 82, no. 2, p. 100–105.

69. MALAQUIAS, J.C., STEICHEN, M., THOMASSEY, M. and DALE, P.J. Electrodeposition of Cu-In alloys from a choline chloride based deep eutectic solvent for photovoltaic applications. *Electrochimica Acta*. 2013. Vol. 103, p. 15–22.

70. DERGACHEVA, M.B., URAZOV, K.A. and PENKOVA, N.V. Electrodeposition of $CuInSe_2$ films onto a molybdenum electrode. *Russian Journal of Applied Chemistry*. 2010. Vol. 83, no. 4, p. 653–658.

71. KASHYOUT, A.E., AHMED, E.Z., MEAZ, T., NABIL, M. and AMER, M. (One-step) electrochemical deposition and characterization of $CuInSe_2$ thin films. *Alexandria Engineering Journal*. 2014. Vol. 53, no. 3, p. 731–736.

72. TANAKA, T., YAMAGUCHI, T., OHSHIMA, T., ITOH, H., WAKAHARA, A. and YOSHIDA, A. Effect of Cl ion implantation on electrical properties of $CuInSe_2$ thin films. *Solar Energy Materials and Solar Cells*. 2003. Vol. 75, no. 1–2, p. 109–113.

73. LIBO, L., YUE, M., GUANXIONG, G., WENTAO, W., SHAOWEN, G., JUN, Y. and JINGCHEN, X. Fabrication and characterization of copper-indium-diselenide ($CuInSe_2$, CIS) thin film using one-step electro-deposition process. *Journal of Alloys and Compounds*. 2016. Vol. 658, p. 774–779.

74. ROCKETT, A. and BIRKMIRE, R.W. $CuInSe_2$ for photovoltaic applications. *Journal of Applied Physics*. 1991. Vol. 70, no. 10, p. 81.

75. PATHAN, H.M. and LOKHANDE, C.D. Chemical deposition and characterization of copper indium diselenide (CISe) thin films. *Applied Surface Science*. 2005. Vol. 245, no. 1–4, p. 328–334.

76. BARI, R.H., PATIL, L.A., SONAWANE, P.S., MAHANUBHAV, M.D., PATIL, V.R. and KHANNA, P.K. Studies on chemically deposited $CuInSe_2$ thin films. *Materials Letters*. 2007. Vol. 61, no. 10, p. 2058–2061.

77. HANKARE, P.P., RATHOD, K.C., CHATE, P., JADHAV, A.V. and MULLA, I.S. Preparation and characterization of $CuInSe_2$ thin films by chemical bath deposition technique. *Journal of Alloys and Compounds*. 2010. Vol. 500, no. 1, p. 78–81.

78. MEGLALI, O., ATTAF, N., BOURAIOU, A., BOUGDIRA, J., AIDA, M.S. and MEDJAHDI, G. Chemical bath composition effect on the properties of electrodeposited $CuInSe_2$ thin films. *Journal of Alloys and Compounds*. 2014. Vol. 587, p. 303–307.

79. SENE, C., CALIXTO, M.E., DOBSON, K.D. and BIRKMIRE, R.W. Electrodeposition of $CuInSe_2$ absorber layers from pH buffered and non-buffered sulfate-based solutions. *Thin Solid Films*. 2008. Vol. 516, no. 8, p. 2188–2194.

80. WELLINGS, J.S., SAMANTILLEKE, P., HEAVENS, S.N., WARREN, P. and DHARMADASA, I.M. Electrodeposition of $CuInSe_2$ from ethylene glycol at 150 °C. *Solar Energy Materials and Solar Cells*. 2009. Vol. 93, no. 9, p. 1518–1523.

81. TAUNIER, S., SICX-KURDI, J., GRAND, P.P., CHOMONT, A., RAMDANI, O., PARISSI, L., PANHELEUX, P., NAGHAVI, N., HUBERT, C., BEN-FARAH, M., FAUVARQUE, J.P., CONNOLLY, J., ROUSSEL, O., MOGENSEN, P., MAHÉ, E., GUILLEMOLES, J.F., LINCOT, D. and KERREC, O. $Cu(In,Ga)(S,Se)_2$ solar cells and modules by electrodeposition. *Thin Solid Films*. 2005. Vol. 480–481, p. 526–531.

82. ASHWINI, R., PRIYANKA, L., GANESH, B., MANORAMA, L. and NANDU, C. Study of electrochemically grown copper indium diselenide (CIS) thin films for photovoltaic applications. *Journal of Materials Science: Materials in Electronics*. 2016. Vol. 27, no. 12, p. 12374–12384.

83. WHANG, T.J., HSIEH, M.T. and KAO, Y.C. Studies of single-step

electrodeposition of $CuInSe_2$ thin films with sodium citrate as a complexing agent. *Applied Surface Science*. 2010. Vol. 257, no. 5, p. 1457–1462.

84. GANCHEV, M., KOIS, J., KAELIN, M., BEREZNEV, S., TZVETKOVA, E., VOLOBUJEVA, O., STRATIEVA, N. and TIWARI, A. Preparation of $Cu(In,Ga)Se_2$ layers by selenization of electrodeposited Cu-In-Ga precursors. *Thin Solid Films*. 2006. Vol. 511–512, p. 325–327.

85. CHANDRAN, R., PANDEY, R. and MALLIK, A. One step electrodeposition of $CuInSe_2$ from an acidic bath: A reduction CO-deposition study. *Materials Letters*. 2015. Vol. 160, p. 275–277.

86. FISCHER, J., SIEBENTRITT, S. and DALE, P.J. Synthesis and Characterization of CuInSe. In : *ECS Transactions*. 2010. p. 129–142.

87. PARK, J.P., KIM, S.K., PARK, J.Y., OK, K.M. and SHIM, I.W. Deposition of $CuInSe_2$ thin films using stable copper and indium-selenide precursors through two-stage MOCVD method. *Bulletin of the Korean Chemical Society*. 2009. Vol. 30, no. 4, p. 853–856.

88. YOON, S.H., SEO, K.W., LEE, S.S. and SHIM, I.W. Preparation of $CuInSe_2$ thin films through metal organic chemical vapor deposition method by using di-μ-methylselenobis(dimethylindium) and bis(ethylisobutyrylacetato) copper(II) precursors. *Thin Solid Films*. 2006. Vol. 515, no. 4, p. 1544–1547.

89. ARTAUD, M.C, OUCHEN, F, MARTIN, L and DUCHEMIN, S. $CuInSe_2$ thin films grown by MOCVD: characterization, first devices. *Thin Solid Films*. 1998. Vol. 324, no. 1–2, p. 115–123.

90. MAHMOUD, F.A., BOSHTA, M. and SAYED, M.H. Correlation between sprayed $CuInSe_2$ thin films properties and deposition temperature. *Journal of Materials Science: Materials in Electronics*. 2012. Vol. 24, no. 2, p. 448–451.

91. TERASAKO, T., INOUE, S., KARIYA, T. and SHIRAKATA, S. Three-stage growth of Cu-In-Se polycrystalline thin films by chemical spray pyrolysis. *Solar Energy Materials and Solar Cells*. 2007. Vol. 91, no. 12, p. 1152–1159.

92. HSU, K., FU, Y., LIN, P., TANG, I. and LIAO, J. Fabrication and Characterization of $CuInSe_2$ Thin Film Applicable for a Solar Energy Light Absorption Material via a Low Temperature Solid State Reaction. *International Journal of Photoenergy*. 2013. Vol. 2013, p. 7.

93. HANAOR, D.A.H., TRIANI, G. and SORRELL, C.C. Morphology and photocatalytic activity of highly oriented mixed phase titanium dioxide thin films. *Surface and Coatings Technology*. 2011. Vol. 205, no. 12, p. 3658–3664.

94. LUO, P., ZUO, R. and CHEN, L. The preparation of $CuInSe_2$ films by combustion method and non-vacuum spin-coating process. *Solar Energy*

Materials and Solar Cells. 2010. Vol. 94, no. 6, p. 1146–1151.

95. YU, Z., YAN, C.P., HUANG, T., HUANG, W., YAN, Y., ZHANG, Y.X., LIU, L., ZHANG, Y.X. and ZHAO, Y. Influence of sputtering power on composition, structure and electrical properties of RF sputtered $CuIn_{1-x}Ga_xSe_2$ thin films. *Applied Surface Science*. 2012. Vol. 258, no. 13, p. 5222–5229.

96. SHAH, N.M., RAY, J.R., PATEL, K.J., KHERAJ, V.A., DESAI, M.S., PANCHAL, C.J. and REHANI, B. Structural, electrical, and optical properties of copper indium diselenide thin film prepared by thermal evaporation method. *Thin Solid Films*. 2009. Vol. 517, no. 13, p. 3639–3644.

97. MERINO, J.M., LEÓN, M., RUEDA, F. and DIAZ, R. Flash evaporation of chalcogenide thin films. *Thin Solid Films*. 2000. Vol. 361, p. 22–27.

98. PARK, S.C., LEE, D.Y., AHN, B.T., YOON, K.H. and SONG, J. Fabrication of $CuInSe_2$ films and solar cells by the sequential evaporation of In_2Se_3 and Cu_2Se binary compounds. *Solar Energy Materials*. 2001. Vol. 69, p. 99–105.

99. KIM, N., JUN, Y. and CHO, G. Se-loss-induced CIS thin films in RTA process after co-sputtering using $CuSe_2$ and $InSe_2$ targets. . 2014. Vol. 9, no. 3, p. 1009–1015.

100. YOSHINO, K., YOKOYAMA, H., MAEDA, K., IKARI, T., FUKUYAMA, A., FONS, P.J., YAMADA, A. and NIKI, S. Optical characterizations of $CuInSe_2$ epitaxial layers grown by molecular beam epitaxy. *Journal of Applied Physics*. 1999. Vol. 86, no. 8, p. 4354.

101. CHICHIBU, S., MIZUTANI, T., MURAKAMI, K., SHIODA, T., KURAFUJI, T., NAKANISHI, H., NIKI, S., FONS, P.J. and YAMADA, A. Band gap energies of bulk, thin-film and epitaxial layers of $CuInSe_2$ and $CuGaSe_2$. *Journal of Applied Physics*. 1998. Vol. 83, no. 7, p. 3678.

102. SHIH, C.H., LO, I., YOU, S.T., TSAI, C.D., TSENG, B.H., CHEN, Y.F., CHEN, C.H. and HSU, G. Direct growth of heteroepitaxial $CuInSe_2$ on GaN (0001) by molecular beam epitaxy. *Thin Solid Films*. 2015. Vol. 574, p. 132–135.

103. RATHKE, B. Mittheilungen aus dem Universitäts-Laboratorium zu Königsberg. XV. Beiträge zur Kenntniss der chemischen Aehnlichkeit von Schwefel und Selen. Selendithionige Säure. Selentrithionsäure. *Journal für Praktische Chemie*. 1865. Vol. 95, no. 1, p. 1–30.

104. FOERSTER, F., LANGE, F., DROSSBACH, O. and SEIDEL, W. Beiträge zur Kenntnis der schwefligen Säure und ihrer Salze. I. Über die Zersetzung der schwefligen Säure und ihrer Salze in wäßriger Lösung. *Zeitschrift für anorganische und allgemeine Chemie*. 1923. Vol. 128, no. 1, p. 245–342.

105. ZELIONKAITĖ, V. and JANICKIS, V. Образование диселенотетратионата

калия при взаимодействии сернистой и селенистой кислот. *Труды Академии наук Литовской ССР*. 1955. Vol. 25, no. 1, p. 841.

106. PAŠAUSKAS, E. and ŠULIAKIENĖ, J. *Труды Академии наук Литовской ССР*. 1961. Vol. 3, no. 26, p. 195–201.

107. JANICKIS, V. *Seleno- ir telūropolitionatai*. Kaunas : Technologija, 2007.

108. SCHULZE, H. Über das Verhalten von seleniger zur schwefliger Säure. *Journal für Praktische Chemie*. October 1885. Vol. 32, no. 1, p. 390–407.

109. ŠUKYTĖ, J. and ZELIONKAITĖ, V. *Журнал Неорганической Химии*. 1958. Vol. 3, no. 8, p. 1755–1760.

110. ZELIONKAITĖ, V., ŽARNAUSKAS, A. and BERNATONIENĖ, L. *Труды Академии наук Литовской ССР*. 1970. Vol. 12, p. 83–91.

111. GMELIN, L and KRAUT, K.J. *Gmelin-Kraut's Handbuch Der Anorganischen Chemie: Unter Mitwirkung Hervorragender Fachgenossen*. Nabu Press, 2010. ISBN 1142582299.

112. ŠUKYTE, J. *Doctoral Thesis*. Kaunas University of Technology, 1973.

113. IVANAUSKAS, R. *Doctoral Thesis*. Kaunas University of Technology, 1995.

114. AUSTAD, T. Studies on polythionates. IV. The action of the cyanide ion on the selenotrithionate ion and the diselenotetrathionate ion in acetonitrile. *Acta Chemica Scandinavica*. 1975. Vol. 29a, no. 1, p. 71–75.

115. NORRIS, J.F. Organic Chemistry. *Journal of the American Chemical Society*. 1901. Vol. 23, no. 8, p. 123–130.

116. HEUER, O. *Doctoral Thesis*. University of Hanover, 1926.

117. FOSS, O. and JAHR, J. Isomorphous Thiosulphates of Divalent Sulphur, Selenium and Tellurium. *Acta Chemica Scandinavica*. 1950. Vol. 4, p. 1560–1566.

118. FOSS, O. and TJOMSLAND, O. The crystal structure of berium selenopentathionate dihydrate. *Acta Chemica Scandinavica*. 1954. Vol. 8, no. 9, p. 1701–1708.

119. ZELIONKAITĖ, V. and ŠUKYTĖ, J. *Труды Академии наук Литовской ССР*. 1966. Vol. 1, no. 36, p. 3–13.

120. ZELIONKAITĖ, V. and JANICKIS, V. *Труды Академии наук Литовской ССР*. 1969. Vol. 3, no. 58, p. 133–137.

121. BAGDONAITĖ, O., SAVICKAS, F. and JANICKIS, V. Материалы конференции по внед-рению результатов научных исследование, проводимых в вузах рес-публики. *Химия и химическая технология*. 1973.

P. 147–150.

122. ZELIONKAITĖ, V. and JANICKIS, V. *Журнал Неорганической Химии*. 1974. Vol. 19, no. 12, p. 3219–3223.

123. ZELIONKAITĖ, V., ŠUKYTĖ, J. and ŠULIAKIENĖ, J. *Труды Академии наук Литовской ССР*. 1963. Vol. 3, p. 93–101.

124. ZELIONKAITĖ, V., ŠUKYTĖ, J. and KUDARAUSKIENĖ, D. *Труды Академии наук Литовской ССР*. 1964. Vol. 1, no. 36, p. 117–126.

125. ZELIONKAITĖ, V., PAŠKAUSKAS, E. and ŠUKYTĖ, J. *Журнал неорганической химии*. 1957. Vol. 2, no. 6, p. 1341–1348.

126. FOSS, O. Displacement Equilibria and Catalysis on Thiosulphates, Xanthates and Dithiocarbamates of Divalent Sulphur, Selenium and Tellurium. *Acta Chemica Scandinavica*. 1949. Vol. 3, p. 1385–1399.

127. ŠUKYTĖ, J. and PADOLSKIS, M. *Труды Академии наук Литовской ССР*. 1963. Vol. 3, p. 103–115.

128. JANICKIS, V. *Doctoral Thesis*. Kaunas University of Technology, 1983.

129. STAMM, H., SEIPOLD, O. and GOEHRING, M. Zur kenntnis der polythionsäuren und ihrer bildung. *Zeitschrift für anorganische und allgemeine Chemie*. 1941. Vol. 247, no. 3, p. 277–306.

130. FOSS, O. and KRINGLEBOTN, I. Displacement of sulfite groups of polythionates by thiosulfate. *Acta Chemica Scandinavica*. 1961. Vol. 15, p. 1608–1609.

131. FOUST, A.S. and JANICKIS, V. The selenotrithionate dianion: crystal and molecular structure of $K_2SeS_2O_6$. *Inorganic Chemistry*. 1980. Vol. 19, no. 4, p. 1063–1064.

132. FOUST, A.S., JANICKIS, V. and MAROY, K. The diselenotetrathionate dianion: preparation and X-ray structures of two crystalline modifications of $[Co(en)_2Cl_2]_2Se_2S_2O_6 \cdot H_2O$. *Inorganic Chemistry*. 1980. Vol. 19, no. 4, p. 1044–1048.

133. BELEVICH, N. N. Synthesis and Optical Properties of $CuInSe_2$ Films. *Inorganic Materials*. 2004. Vol. 40, no. 7, p. 782–787.

134. ZELIONKAITĖ, V. and ŽARNAUSKAS, A. The investigation of diffusion of interaction products between dilute. *Chemical Technology*. 2001. Vol. 18, no. 1, p. 56–60.

135. ZELIONKAITE, V. *Doctoral Thesis*. Kaunas University of Technology, 1964.

136. ŠULIAKIENĖ, J. *Doctoral Thesis*. Kaunas University of Technology, 1964.

137. ATKINS, P. and PAULA, J. *Elements of Physical Chemistry*. 6th Editio. Oxford : Oxford University Press, 2013. ISBN 1429287322.

138. ŠUKYTE, V.J., IVANAUSKAS, R. and JANICKIS, V. Preparation and some properties of Cu–Te–S thin films on the polyamide (PA) surface. *Polish Journal of Chemistry*. 2005. Vol. 79, no. 4, p. 759–771.

139. ZINGARO, R. and COOPER, C. *Selenium*. Van Nostrand Reinhold Company, 1973.

140. MALMSTEN, G., THOREN, I., HOGBERG, S., BERGMARK, J., KARLSSON, S. and REBANE, E. Selenium compounds studied by means of ESCA. *Physica Scripta*. 1971. Vol. 3, no. 2, p. 96–100.

141. ЛИДИН, Р.А., МОЛОЧКО, В.А. and АНДРЕЕВА, Л.Л. *Справочник по неорганической химий*. 1987.

142. MARSH, R.E., PAULING, L. and MCCULLOUGH, J.D. The crystal structure of β selenium. *Acta Crystallographica*. 1953. Vol. 6, no. 1, p. 71–75.

143. EFFENBERGER, H. and PERTLIK, F. Ein beitrag zur Kristallstruktur von α–CuSe (Klockmannit). *Neues Jahrbuch Fur Mineralogie-Monatshefte*. 1981. Vol. 143, no. 1, p. 197–205.

144. EARLEY, J.W. Description and synthesis of the selenide minerals. *American Mineralogist*. 1950. Vol. 35, p. 337.

145. UENO, Y., KAWAI, H., SUGIURA, T. and MINOURA, H. Electrodeposition of $CuInSe_2$ films from a sulphate bath. *Thin Solid Films*. 1988. Vol. 157, no. 1, p. 159–168.

146. STEVELS, A.L.N. and JELLINEK, F. Recueil des Travaux Chimiques des Pays-Bas. *Journal of the Royal Netherlands*. 1971. Vol. 90, no. 3, p. 273.

147. SLAVNOVA, G.K. *Russian Journal of Inorganic Chemistry*. 1963. Vol. 8, p. 1161.

148. CHERIN, P. and UNGER, P. The crystal structure of trigonal selenium. *Inorganic Chemistry*. 1967. Vol. 6, no. 8, p. 1589–1591.

149. NELSON, A.J., SWARTZLANDER, A.B., TUTTLE, J.R., NOUFI, R., PATEL, R. and HÖCHST, H. Photoemission investigation of the electronic structure at polycrystalline $CuInSe_2$ thin-film interfaces. *Journal of Applied Physics*. 1993. Vol. 74, no. 9, p. 5757.

150. NELSON, A.J., FRIGO, S.P. and ROSENBERG, R. Valency and type conversion in $CuInSe_2$ with H_2 plasma exposure: A photoemission investigation. *Journal of Applied Physics*. 1993. Vol. 73, no. 12, p. 8561.

151. SOBOL, P.E., NELSON, A.J., SCHWERDTFEGER, C.R., STICKLE, W.F.

and MOULDER, J.F. Single Crystal $CuInSe_2$ Analysis by High Resolution XPS. *Surface Science Spectra*. 1992. Vol. 1, no. 4, p. 393.

152. CAHEN, D., IRELAND, P.J., KAZMERSKI, L.L. and THIEL, F.A. X-ray photoelectron and Auger electron spectroscopic analysis of surface treatments and electrochemical decomposition of $CuInSe_2$ photoelectrodes. *Journal of Applied Physics*. 1985. Vol. 57, no. 10, p. 4761.

153. ERTL, G., HIERL, R., KNÖZINGER, H., THIELE, N. and URBACH, H.P. XPS study of copper aluminate catalysts. *Applications of Surface Science*. 1980. Vol. 5, no. 1, p. 49–64.

154. JOLLEY, J.G., GEESEY, G.G., HANKINS, M.R., WRIGHT, R.B. and WICHLACZ, P.L. Auger electron and X-ray photoelectron spectroscopic study of the biocorrosion of copper by alginic acid polysaccharide. *Applied Surface Science*. 1989. Vol. 37, no. 4, p. 469–480.

155. KAZMERSKI, L.L., JAMJOUM, O., IRELAND, P.J., DEB, S.K., MICKELSEN, R.A. and CHEN, W. Initial oxidation of $CuInSe_2$. *Journal of Vacuum Science and Technology*. 1981. Vol. 19, no. 3, p. 467.

156. FAUR, M., FAUR, M., JAYNE, D.T., GORADIA, M. and GORADIA, C. XPS investigation of anodic oxides grown on p-type InP. *Surface and Interface Analysis*. 1990. Vol. 15, no. 11, p. 641–650.

157. SAKANE, G. and SHIBAHARA, T. Synthesis and characterization of the cubane-type molybdenum-indium mixed-metal cluster $[Mo_3InS_4 \cdot 2(H_2O)_{10}]^{3+}$. *Inorganic Chemistry*. 1993. Vol. 32, no. 6, p. 777–778.

158. GATES, B., MAYERS, B., CATTLE, B. and XIA, Y. Synthesis and Characterization of Uniform Nanowires of Trigonal Selenium. *Advanced Functional Materials*. 2002. Vol. 12, no. 3, p. 219.

159. EL-SAYED, S.M. Optical investigations of the indium selenide glasses. *Vacuum*. 2003. Vol. 72, no. 2, p. 169–175.

160. BHUVANESWARI, P. V., RAMAMURTHI, K., RAMESH BABU, R. and MOORTHY BABU, S. Structural, morphological, optical and electrical properties of $Cu_{0.87}Se$ thin films coated by electron beam evaporation method. *Applied Physics A*. 2015. Vol. 120, no. 3, p. 1113–1120.

LIST OF PUBLICATIONS AND PROCEEDINGS ON THE TOPIC OF DISSERTATION:

Publications corresponding to the list of Thomson ReutersTM Web of Science database:

1. ŠUKYTE, J., IVANAUSKAS, A. and ANCUTIENĖ, I. Comparative study of selenopolythionic acids $H_2Se_nS_2O_6$ as precursors for formation of chalcogenides layers. *Chalcogenide Letters*. 2015. Vol. 12, no. 11, p. 569–578.
2. IVANAUSKAS, A., IVANAUSKAS, R. and ANCUTIENĖ, I. The deposition of CuInSe2 layer on glass substrate by silar method. *Chalcogenide letters*. 2016. Vol. 13, no. 8, p. 373–380.

Publications in Proceedings of Conferences:

1. IVANAUSKAS, A., ANCUTIENĖ, I., IVANAUSKAS, R. and SAMARDOKAS, L. Selenium containing precursor for semiconducting materials. *Advanced materials and technologies.* Palanga, Lietuva, rugpjūčio 27–31, 2013. p. 72.
2. ŠUKYTĖ, J., IVANAUSKAS, A. and ANCUTIENĖ, I. Comparitive study of selenopolythionic acids $H_2Se_nS_2O_6$ as precursors for formation of chalcogenides layers. *Chemistry and chemical technology.* Kaunas, Lietuva, balandžio 25, 2014. p. 124–127.
3. BAKUTYTĖ, A., IVANAUSKAS, R., IVANAUSKAS, A. and ANCUTIENĖ, I. XRD studies of copper sulfide layers on glass. *Chemistry and chemical technology 2015.* Vilnius, Lietuva, sausio 23, 2015. p. 62–64.
4. IVANAUSKAS, A. and ANCUTIENĖ, I. XPS studies of Cu-In-Se layers on glass. *Chemistry and chemical technology*. Vilnius, Lieruva, balandžio 28–29, 2016. p. 207.
5. IVANAUSKAS, A., IVANAUSKAS, R. and ANCUTIENĖ, I. XRD studies of copper and indium selenide layers on glass. *Chemistry and chemical technology 2017*. Kaunas, Lietuva, balandžio 28, 2017. p. 68.

Publications not included in the thesis:

1. IVANAUSKAS, A., ŠULČIŪTĖ, A. and VALATKA, E. Photoelectrochemical activity of electrophoretically deposited zinc oxide

coatings on stainless steel substrates. *Chemija : mokslo darbai*. 2013. Vol. 24, no. 2, p. 97–102.

2. IVANAUSKAS, R., SAMARDOKAS, L., ANCUTIENĖ, I. and IVANAUSKAS, A. Study of formation and phase composition of thallium selenide layers on polycaproamide. *Materials science*. 2015. Vol. 21, no. 1, p. 13–17.

SL344. 2017-01-09, 10,75 leidyb. apsk. l. Tiražas 12 egz. Užsakymas 14.
Išleido Kauno technologijos universitetas, K. Donelaičio g. 73, 44249 Kaunas
Spausdino leidyklos „Technologija“ spaustuvė, Studentų g. 54, 51424 Kaunas